Journal of Alloys and Compounds 895 (2022) 162450

Contents lists available at ScienceDirect

Journal of Alloys and Compounds

journal homepage: www.elsevier.com/locate/jalcom

Review on chromium coated zirconium alloy accident tolerant fuel cladding

Jianqiao Yang[a,b,*], Martin Steinbrück[b], Chongchong Tang[b], Mirco Große[b], Junkai Liu[a,b], Jinming Zhang[a], Di Yun[a], Shuzhong Wang[a]

[a] Key Laboratory of Thermo-Fluid Science and Engineering of MOE, School of Energy and Power Engineering, Xi'an Jiaotong University, Xi'an 710049, PR China
[b] Institute for Applied Materials, Karlsruhe Institute of Technology, Karlsruhe 76344, Germany

ARTICLE INFO

Article history:
Received 22 August 2021
Received in revised form 19 October 2021
Accepted 20 October 2021
Available online 31 October 2021

Keywords:
Chromium
Coating
Zirconium alloy
Cladding
Accident tolerant fuel

ABSTRACT

The Fukushima-Daiichi accident revealed that the zirconium fuel claddings have the significant safety risk of hydrogen detonation due to the strong oxidation and hydrogen release during the design basis accidents (DBA) and beyond design basis accidents (BDBA). Therefore, research and development of accident tolerant fuel (ATF) concepts that aim to improve nuclear fuel safety during normal operation, operational transients and possible accident scenarios have been boosted in the last decade. Deposition of protective coatings on Zircaloy cladding tubes has been considered as a near-term solution of enhanced ATF cladding. Among the candidate coating materials, there is no doubt that the research progress of Cr coating is the fastest around the world because of the advantages of such type of coating: excellent good chemical stability (including oxidation resistance and hydrothermal corrosion resistance), low thermal neutrons absorption cross-section, and excellent adherent. In this paper, the oxidation, diffusion, and mechanical properties of Cr-coated Zr alloys in normal operation conditions and accident conditions of nuclear reactors are reviewed. The factors that cause the failure of the coating are analyzed, and some questions that need to be clarified and further studied are proposed.

Contents

* Corresponding author at: Key Laboratory of Thermo-Fluid Science and Engineering of MOE, School of Energy and Power Engineering, Xi'an Jiaotong University, Xi'an 710049, PR China.
E-mail address: jianqiao.yang@aliyun.com (J. Yang).

https://doi.org/10.1016/j.jallcom.2021.162450
0925-8388/

1. Introduction

The energy density of a light water reactor (LWR) core is up to 50–75 MW/m^3, and the thermal power of a standard LWR reactor can reach to 3000 MW [1]. For example, it was calculated that there is about 0.2% heat remaining as decay heat in the reactor core after the reactor was stopped for ten days [2]. Once the coolant of the reactor is lost, the temperature of the reactor core sharply increases. The Zircaloy cladding tubes undergo extensive oxidation in the steam-containing atmosphere, resulting in degradation of the claddings and generation of hydrogen and heat.

Owing to the relatively good oxidation resistance, excellent neutron irradiation resistance, good ductility, and low thermal neutron absorption cross-section, Zircaloy have been chosen as cladding materials for UO_2 fuel since 1950. The Fukushima nuclear accident revealed that the zirconium fuel cladding materials have the significant safety risk of hydrogen detonation due to the fast and strong oxidation during the DBA and BDBA. Since then, the concept of accident tolerant fuel (ATF) cladding was put forward, aiming to strengthen the oxidation resistance of the cladding materials, to reduce the temperature increasing, the hydrogen releasing and to prolong the coping time during accident [3]. ATF cladding materials should strongly decrease the risk of temperature escalation during loss of the coolant accidents (LOCA), and increase the coping time for plant operators to recover from the accident [4–7]. There are two development directions of ATF cladding materials. One is to prepare a coating on the surface of the Zircaloy tubes, and the other is to develop new cladding materials to replace Zr alloys There is no doubt that it takes a long period to develop and verify a new type of cladding materials. The advantages of preparing a protective coating on fuel cladding tubes is that the coating can significantly improve the oxidation resistance of the cladding during LOCA and has little effect on the original fuel component design, reactor structure design and water chemistry. Deposition of protective coatings on Zircaloy cladding tubes has been considered as a near-term solution of enhanced ATF cladding [8,9].

Up to now, many types of coating materials have been developed, including MAX phase coatings [10–14], carbide coatings [15,16], nitride coatings [17–20], pure metal coatings [21–26] and alloy coatings [27–32]. Previous studies show that MAX phase coatings such as Ti-Al-C and Cr-Al-C are susceptible to cracking through the coating during heat treatment, water corrosion, and high temperature steam oxidation [33,34]. SiC coatings are unstable at 350 °C / 20 MPa due to dissolution of corrosion products [35]. Moreover, SiC coating may crack under the thermal shock because of its high brittleness. Metal nitride coatings such as CrN decompose into Cr_2N and N_2 at temperatures from 500 °C to 975 °C, resulting in the formation of cracks [36,37]. For the FeCrAl coating, the Fe-Zr eutectic temperature is about 900 °C, which is obviously lower than the typical LOCA temperature [38–41]. Compared with other coatings, there are several advantages for the chromium coating.

- The oxidation resistance of the Cr coating is excellent because of the compact Cr_2O_3 film formed on the coating surface during LOCA. The parabolic rate constant in mg·cm^{-2}·s$^{-0.5}$ Researches of Cr coating and Zry-4 in steam at 1200 °C is 0.05 [42] and 1.09 [43], respectively.
- The adhesion property of the Cr coating is excellent. No coating spallation was found on the Cr coated Zr alloys after the deformations such as thermal expansion, ballooning, or irradiation growth of the cladding tube under normal operation conditions or accident condition including quenching of overheated fuel rods [44].
- The thermal neutron absorption cross-section of Cr, 2.9 barn, is relatively lower than that of other alternative coating materials.
- The elastic modulus of Cr is about twice that of Zr, which helps to improve the overall stiffness of the cladding [45].
- The Cr-Zr eutectic temperature is about 1332 °C [46], which is higher than the design basis accident temperatures, but, on the other hand, determines the upper temperature limit for the protective effect of the coating during severe accidents.
- The wettability of Cr coating is higher than that of Zircaloy, which can improve thermal-hydraulic performance of the cladding [47].

In this paper, the oxidation, diffusion, and mechanical properties of Cr-coated Zr alloys in normal operation conditions and accident conditions are reviewed. The factors that lead the failure of the coating is analyzed, and some questions that need to be clarified and further studied are proposed.

2. Hydrothermal corrosion behavior

Although Cr coated Zr alloys were developed to enhance the oxidation resistance of the cladding materials under accident conditions, the coated cladding should provide the same or better properties as conventional cladding during the long-term normal operation in-high temperature and high-pressure aqueous environment. In this section, current research results about the performance of Cr coated Zr alloys under normal operation conditions are summarized.

For normal operation conditions, most of the reported corrosion tests were done in pressurized water at 360 °C and 18.6 MPa [42,44,48–51], which corresponds to typical operation environment of pressurized water reactors (PWR). Also, in consideration of the duration of the experiment, some tests were done in pressurized water or steam environment at temperatures from 250 °C to 500 °C [52–54].

The PWR aqueous environment is a subcritical water environment, therefore the mode of occurrence of Cr, including unreacted

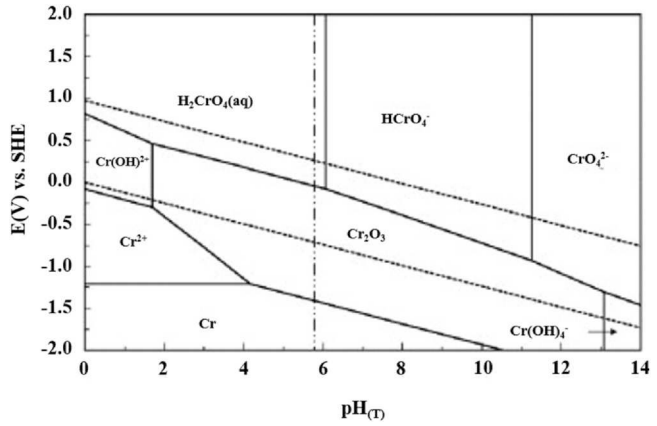

Fig. 1. Pourbaix diagrams for Cr at 350 °C, 25 MPa and 10^{-6} mol/kg. Reproduced with permission from Ref. [55].

Cr, Cr oxides or soluble ions, can be predicted by the Pourbaix diagrams. Fig. 1 shows the Pourbaix diagram for Cr at 350 °C, 25 MPa and 10^{-6} mol/kg [55]. It is known that the electrochemical potential and pH value of the water environment in PWR reactor are about −0.5 V_{SHE} and 7.0, respectively. Obviously, it is indicated that a stable Cr_2O_3 layer would form under normal operation conditions, which was confirmed by several researches on the corrosion behavior of pure Cr metal [56] and Ni-Cr alloys in sub and supercritical water environment [57–60].

Fig. 2 summarizes the visual appearance of some Cr coated Zr alloy specimens after steam or high pressure water tests. It can be seen that most of the sample surfaces show golden colors, which suggests that the thickness of the Cr_2O_3 layer on the specimens' surface is about some hundreds of nanometers [48] (considering the fact that the wavelength of yellow is about 580–596 nm). Moreover, there are no cracks or delamination of the Cr coatings after tests. No exacerbated Zr alloy corrosion was found at the scratch locations even though the specimen was intentionally scratched on the surface [48]. Brachet et al. [52] also performed a similar experiment to investigate the effect of pre-existing cracks on the oxidation resistance of a PVD coated sample. After exposure under PWR conditions, a tiny zone of ZrO_2 formed under the crack and no spallation or cracks of coating were found. The appearance of the Cr-coated specimens after corrosion tests in high-temperature aqueous environment confirms that the Cr coating survived after exposure in PWR environment, and the coating had a "self-healing" effect for some tiny pits or cracks on the coating surface. The weight gain data also support the visual results. Fig. 3 shows the weight gain of different kinds of Zr alloys with and without Cr coatings exposed in simulated PWR environment at 360 °C. All the samples shown in Fig. 3 are cubic specimens and are coated in both sides. It can be seen that the weight gain of the coated samples is considerably lower than that of the uncoated ones. The oxidation rate of the Cr coated samples was observed to be the highest at the beginning of the exposure, then levelled off at very low rates afterward. In summary, the weight gain of Cr coated Zr alloys after exposure in pressurized water at 360 °C is about 0.05 mg/cm^2 after 180 days exposure. The coating fabrication methods had little effect on the weight gain.

The impact of irradiation on the corrosion behavior of the coating in normal operation conditions should be figured out before licensing. Framatome started the first irradiation of Cr-coating in a commercial PWR, the Gösgen reactor, in 2016 [61]. The objective of this project is to evaluate the microstructure, the corrosion kinetics and the integrity of Cr coated $M5_{Framatome}$ cladding under prototypical irradiation. The first feedback from this project had been announced in the Nuclear Materials Conference 2020 (NuMat 2020). After 3 cycles' irradiation, the Cr coating is adherent and exhibits similar behavior under irradiation as already had been observed out-of-pile. Except that, an irradiation test of Cr coated claddings began in 2018 by Idaho National Laboratory. Up to now, six irradiation cycles have been completed. Some results of this experiment had been announced in the 10th annual EPRI/DOE/INL Joint Accident Tolerant Fuel Workshop in 2021.

3. Oxidation behavior under accident conditions

In DBA situations, the core temperature can rapidly increase up to 1200 °C due to the stored heat in the pellets cannot be carried away by coolants, then decreases because of the decreasing of decay heat and later the re-injection of coolants. During the temperature increasing process, the oxidation resistance of the coating is one of the key performance indicators to evaluate the quality of the coating. The oxide films formed outside the coating should be chemically stable in steam environment to limit the diffusion of O, OH, and also of hydrogen to the underlying Zr substrate. Moreover, when the coolant was re-injected into the reactor, the coating should be physically stable (no thermo-shock induced fracture such as cracks, shedding or obvious deforming). In this section, the oxidation kinetics and the degradation mechanism of Cr coated Zr alloys under accident conditions are reviewed.

3.1. Reactions and oxidation kinetics

The oxidation behavior of chromium in steam environment at high temperatures is different with that in pure oxygen or dry air

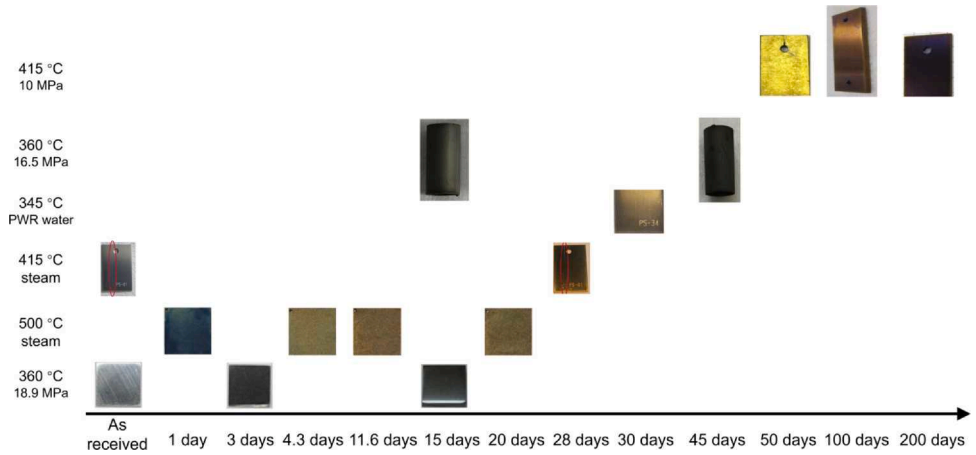

Fig. 2. Visual aspects of Cr coated Zr alloy specimens after steam or high pressure water tests. Reproduced with permission from Ref [42,44,48,51–53].

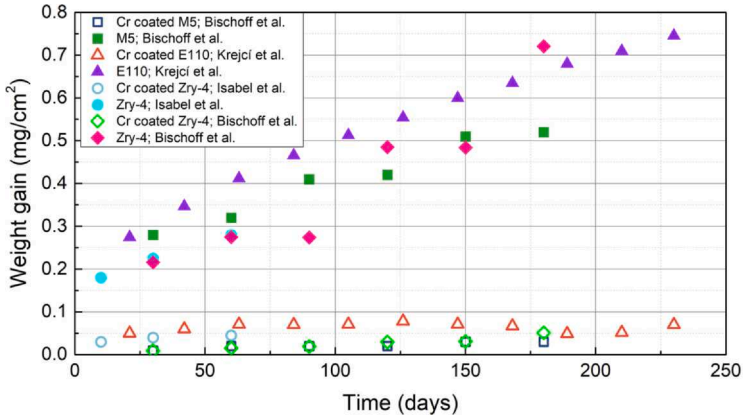

Fig. 3. Weight gain of Zr alloys and Cr-coated Zr alloys samples exposed in simulated PWR environment at 360 °C.

environment. Especially, the existence of nitrogen can affect the oxidation kinetics of Cr coating [62]. The possible reactions between Cr and oxidizing agents for the formation of Cr oxide and Cr oxyhydroxide under wet oxygen or steam environment are shown as follows [63–65]:

$$Cr(s) + \frac{3}{4}O_2(g) \rightarrow \frac{1}{2}Cr_2O_3(s) \quad (1)$$

$$\frac{1}{2}Cr_2O_3(s) + \frac{3}{4}O_2(g) \rightarrow CrO_3(g) \quad (2)$$

$$2Cr(s) + 3H_2O(g) \rightarrow Cr_2O_3(s) + 3H_2(g) \quad (3)$$

$$\frac{1}{2}Cr_2O_3(s) + H_2O(g) + \frac{3}{4}O_2(g) \rightarrow CrO_2(OH)_2(g) \quad (4)$$

$$\frac{1}{2}Cr_2O_3(s) + \frac{1}{2}H_2O(g) + \frac{1}{2}O_2(g) \rightarrow CrO_2(OH)(g) \quad (5)$$

Some volatile Cr oxides (CrO_3) or volatile Cr oxyhydroxides ($CrO_2(OH)_2$ or CrO_2OH)) can form at high temperature. The formation of volatile products depends on both the steam and oxygen partial pressure. The reaction (4) is expected to dominate up to 900 °C, and the reaction (5) is the main reaction at temperatures higher than 1300 °C [64]. The formation of volatile Cr oxyhydroxides usually occurs at the grain boundaries at first. For instance, a porous sintered-like Cr_2O_3 layer was formed on a Cr coated Zr alloy sample after a thermal shock test (the samples were annealed in vacuum environment for 10 min at 1200 °C with quenching into boiled water). The authors deduced that the formation of pores on the coating surface is owing to the formation of volatile $CrO2(OH)_2$ in water during the quenching process [66]. The volatilization of Cr oxides or oxyhydroxide may lead to the irregular consumption of the Cr coatings under LOCA scenario. Royer et al. [62] found that the weight loss caused by volatilization of Cr oxides or oxyhydroxides in air at 1300 °C was about 0.04 mg/cm^2·h^1, which is two orders of magnitude lower than the weight gain by formation of Cr_2O_3 at the same environment. in other words, compared with the growth of Cr_2O_3 layer, the volatilization of Cr oxides or oxyhydroxides is not the main process during the LOCA transient. Similar phenomenon was also discussed and confirmed by Brachet et al. [67] in a series of steam oxidation tests of Cr coated Zr alloys at temperatures up to 1300 °C. Yeom et al. [68] found that the growth kinetics of a Cr coated Zr alloy specimen in steam environment at 1230 °C did not perfectly obey a parabolic law, and they speculated that the irregular growth kinetics of the Cr_2O_3 layer was due to the volatilization of the oxidation products. Nevertheless, the in-situ detection of volatile Cr oxides or oxyhydroxide during a high temperature oxidation experiment in simulated LOCA conditions is challenging. Groβe et al. [69] investigated the corrosion behavior of Cr_2O_3 under operational and LOCA conditions. They measured a corrosion rate of compact Cr_2O_3 of 45.2 ± 13.7 µm/year in static autoclave tests performed at IIT. For high porosity Cr_2O_3 a much higher corrosion rate was found. A mass loss of 0.57 mg/cm^{2}h^1 was determined after an isothermal steam oxidation test at 1200 °C for compact Cr_2O_3.

It is known that the oxidation kinetics of pure Cr in oxygen-containing steam environment show parabolic behavior [70]. The growth of the Cr_2O_3 layer is governed by diffusion of chromium ions through the Cr_2O_3 lattice, and additionally by the diffusion of oxygen along grain boundaries to the oxide/metal interface. Fig. 4(a) shows the mass gain of three types of Cr coated Zr alloy samples in steam environment at 1200 °C, performed by a thermogravimetry at KIT [71]. As a representative, the work shows that the oxidation kinetics of both Cr-coated Zr alloys obeys parabolic laws until the transition process finished. The transition and the degradation mechanism of the Cr coating will be discussed in the nest section. Besides, a 500–1200 °C transition test on both the coated and uncoated Zr alloys shows that the oxidation rates of the Cr coated Zr alloys are significantly reduced compared to that of the uncoated ones (Fig. 4(b)).

The high-temperature oxidation kinetics of Cr-coated Zr alloys in steam or wet air environment at the temperature range of 600–1400 °C, relevant for LOCA scenarios, have been extensively investigated by several labs. Usually, a parabolic equation was used to describe the mathematic relation between the oxide thickness and the oxidation duration:

$$\delta = \sqrt{k_p \times t} \quad (6)$$

Where $\delta$is the thickness of the oxides with the unit of m, k_p is the kinetics constant in m^2/s, and t is the exposure time in seconds. The kinetics constant is a temperature-controlled value, which can be described by Arrhenius equations. The value of k_p is affected by the coating characteristics (compactness, crystal texture and defects) and oxidation environments (steam, simulated steam, dry air or wet air). Tube samples with coating on only one side were used by several researchers to test the oxidation behavior. It is hard to compare the oxidation rate between the two sides coated samples and the one side coated sample because of the significant oxidation of the un-coated Zr alloy side. Table 1 summarizes the thicknesses of Cr_2O_3 layer on different Cr coated Zr alloy samples after oxidation in simulated LOCA conditions. It can be seen that the thicknesses of the Cr coating prepared by cold spraying, plasma spraying or 3D printing could be higher than 50 µm, while the thickness of the PVD coating is usually lower than 15 µm. However, the oxidation rate of the magnetron sputtered samples is lower than that of the Cr coated samples prepared by other methods.

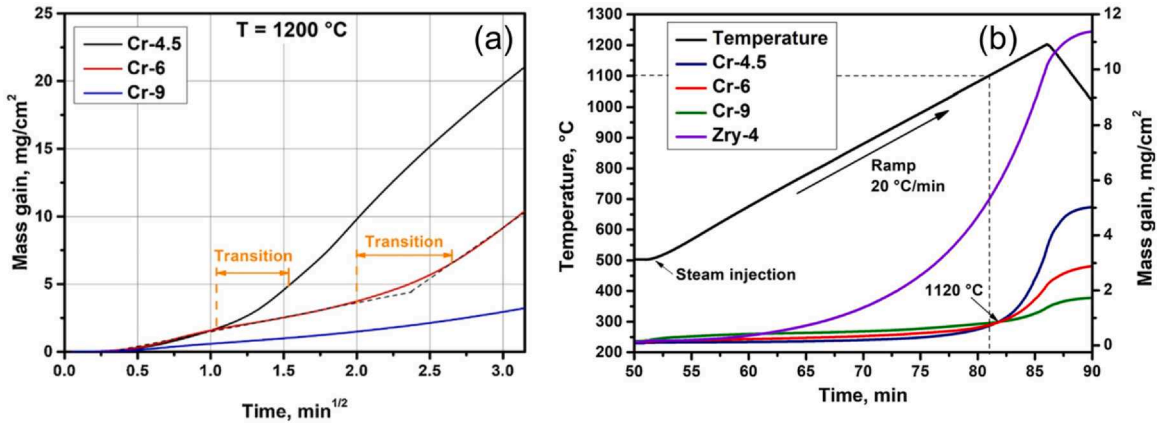

Fig. 4. (a) Weight gain of three types of Cr-coated Zr alloys samples exposed in steam environment at 1200 °C. Parabolic laws were found on the growth kinetics of the coating at the beginning. Then, the coating gradually lost its protectiveness (corresponding to the transition zone in the figure). (b) Weight gain of three types of Cr-coated Zr alloys samples during the transient test of Cr-coated and uncoated Zr alloys in steam environment at 500–1200 °C. Reproduced with permission from Ref [71].

Table 1
Summarization of the thickness of oxide film of Cr coated Zr alloys after exposure in simulated LOCA conditions.

Coating method	Coating thickness (μm)	Temperature (°C)	Exposure time (min)	Environment	Oxide thickness (μm)	Refs
Magnetron sputtering	12–15	1000	300	Steam	~3	[21]
Magnetron sputtering	12–15	1100	300	Steam	6–7	[21]
Magnetron sputtering	5–10	1200	5	Steam	2.8	[42]
Magnetron sputtering	8	1000	60	Steam	2.9	[22]
Magnetron sputtering	8	1100	60	Steam	4.9	[22]
Magnetron sputtering	8	1200	60	Steam	5	[22]
Magnetron sputtering	8	1200	15	Steam	3	[22]
Magnetron sputtering	8	1200	30	Steam	2.5	[22]
3D laser	80	1200	33.3	Steam	< 4	[44]
Magnetron sputtering	10.6 ± 0.6	1200	30	Steam	4–4.5	[72]
Cold spraying	27	1200	90	Steam	9.2	[53]
Laser scanning	~100	1200	33.3	Steam	Several micrometers	[23]
Arc ion coating	10	1200	33.3	Steam	< 10	[73]
Cold spraying	50–60	1310	90	Steam	9	[68]
Vacuum arc plasma deposition	~30	800	60	Air	1–2	[25]
Vacuum arc plasma deposition	~30	1000	60	Air	2–3	[25]
Vacuum arc plasma deposition	~30	1200	60	Air	12	[25]
Air plasma spray	70	1200	60	Steam	7	[24]
Multi arc ion coating	2	1060	60	Air	0.8	[74]

3.2. Degradation mechanism of the Cr coating by oxidation reaction (below the Cr-Zr eutectic temperature)

The aim of developing Cr-coated Zr alloy ATF cladding materials is to improve the oxidation resistance of the cladding materials, and make it possible to tolerate the LOCA environment for a considerably longer period than the existing fuel designs. The time during which the coatings survive in beyond design basis severe accident conditions is a key parameter to evaluate the coating quality. Although parabolic laws were obtained for the growth of Cr_2O_3 film on the Cr coated Zr alloys in accident conditions, the survival time of the coating cannot be simply calculated according to a parabolic equation and a coating thickness because that breakaway oxidation may occur before the coating was totally consumed. In this section, two degradation mechanisms of the Cr coating by oxidation reaction in LOCA conditions are introduced. The degradation mechanisms of the Cr coating to be introduced in this section are limited into design-based accidents, and the degradation due to the Cr-Zr eutectic reaction will be discussed in the subsequent section.

A degradation mechanism of Cr coated Zr alloys in LOCA conditions based on the inward diffusion of oxygen along the ZrO_2 particles which distributed on Cr grain boundaries was proposed by Brachet et al. [67], as shown in Fig. 5.

Step 1: At the initial stage, a Cr_2O_3 layer and a Zr-Cr interlayer are formed. The Zr atoms from the Zr substrate went through the Zr-Cr interlayer and diffused along the Cr grain boundaries.

Step 2: At the middle stage, the inward diffused oxygen contacts with the Zr atoms in the Cr grain boundaries, resulting in the formation of ZrO_2 stringers, which are detrimental because they can form a continuous network of ZrO2 at Cr grain boundaries and promote the diffusion of oxygen anions. It should be mentioned that the ZrO_2 particles on the Cr grain boundaries has been observed by TEM, as shown in Fig. 6(b). The formation of the ZrO_2 on the Cr grain boundaries led to the loss of protectiveness of the residual Cr coating: oxygen would diffuse via the newly formed ZrO_2 paths and no longer reacted with the residual Cr coating.

Step 3: At the end stage, the inward diffused oxygen reaches the Zr-Cr interlayer and the Zr substrate. Then, the Zr substrate is oxidized, and the protectiveness of the Cr coating is totally lost. The structure of the heavily oxidized Cr coated Zr alloy, shown in Fig. 6(a), includes a cracked Cr_2O_3 layer, a residual Cr coating layer with ZrO_2 embedded in the Cr grain boundaries, a Cr-Zr interlayer, a ZrO_2 layer and an α-Zr(O) layer and a prior β-Zr substrate.

The degradation mechanism proposed by Brachet et al. [67] is based on TEM and EBSD analyses of the oxidized Cr coated samples. The formation of the embedded ZrO_2 in Cr grain boundaries and the

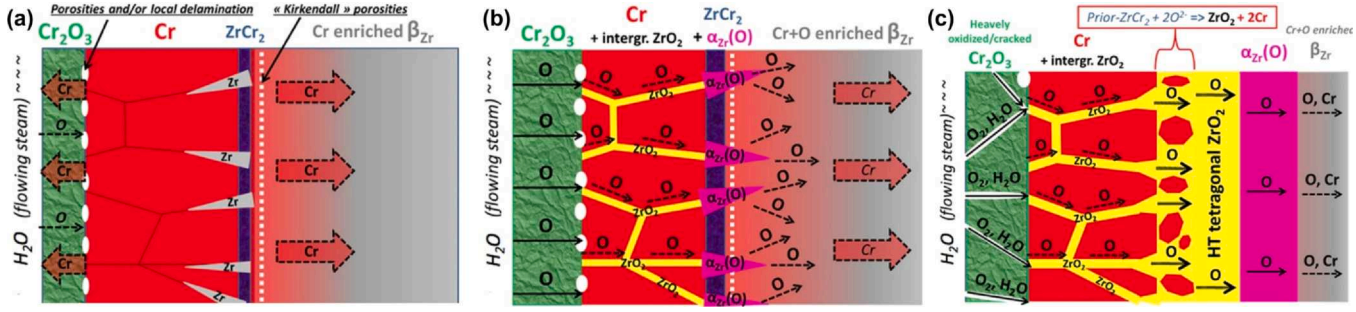

Fig. 5. Schematic of the degradation mechanism of Cr coated Zr alloys in high temperature steam environment proposed by Brachet et al. Reproduced with permission from Ref. [67].

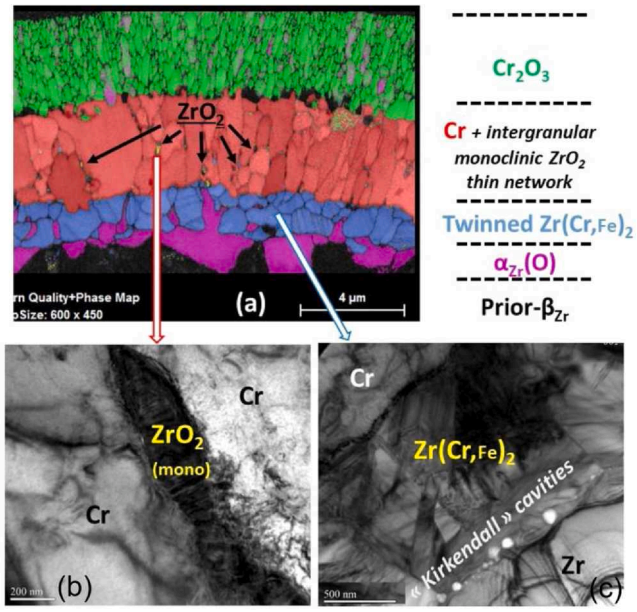

Fig. 6. Typical microstructure of a Cr-coated Zircaloy-4 sample after steam oxidation for 1400 s at 1200 °C. (a) SEM-EBSD phase map. (b) and (c) is TEM micrograph. Reproduced with permission from Ref [67].

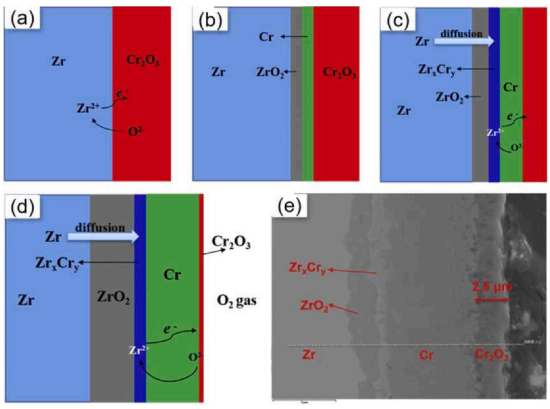

Fig. 7. Schematic of the degradation mechanism of Cr coated Zr alloys in high temperature steam environment proposed by Han et al. The mechanism is based on the premise that the Cr_2O_3 layer is completely formed. Reproduced with permission from Ref. [22].

twin crystal $Zr(Cr, Fe)_2$ can be considered as the evidences for this mechanism. Generally, the Cr_2O_3 layer is compact and protective, which is able to inhibit further oxidation and hydrogen embrittlement of the inner side of coatings.

Another possible degradation mechanism of Cr coated Zr alloys in LOCA conditions based on the reduction of Cr_2O_3 and re-formation of Cr was proposed by Han et al. [22], as shown in Fig. 7.

Step 1: The Cr coating was totally oxidized, and a Cr_2O_3 layer formed. O^{2-} gradually diffused through the Cr_2O_3 layer. Meanwhile, e^- diffused outward, resulting in the formation of Zr^{4+}.

Step 2: The inward diffused O^{2-} contacted with Zr^{4+} in the Zr substrate to form ZrO_2. The outward diffusion of e^- led to the reduction of Cr_2O_3, forming a Cr layer again.

Step 3: The newly formed Cr diffused inward, and Zr atoms diffused through the ZrO_2 layer to form Zr_xCr_y with the inward diffused Cr atoms. Meanwhile, e^- was kept transferring from the Zr substrate to the Cr_2O_3 layer, resulting in the continuous growth of the Cr layer and the ZrO_2 layer.

Finally, a stable structure with a Cr_2O_3 layer, a newly formed Cr layer, a Cr-Zr diffusion layer, a ZrO_2 inner oxidation layer and a Zr substrate layer were formed, as shown in Fig. 7(d). This structure is consistent with the observed Cr coated Zr alloy sample after oxidation in steam environment at 1200 °C for 30 min, as shown in Fig. 7(e).

The reaction that Cr_2O_3 can be reduced by the outward diffused Zr is a key process of the degradation mechanism of the Cr coating. Once the Cr_2O_3 is reduced, the newly formed Cr will be oxidized to Cr_2O_3 again. The thickness of the Cr_2O_3 remain unchanged when the oxidation reaction rate of Cr and the reduction reaction rate of Cr_2O_3 reaches a balance [75]. During that stage, whether the Cr_2O_3 layer is protective is doubtable. Moreover, even though the balance is reached, the diffusion and dissolution of Cr atoms in the Zr substrate cannot be stopped. As a result, the thickness of the Cr_2O_3 layer keeps decreasing and the breakaway oxidation reaction of the Zr substrate finally occurs [76]. Nevertheless, none of the researchers focused on how the Cr_2O_3 layer loses its protectiveness. Both mechanisms are based on the precondition that H_2O/oxygen from the atmosphere can easily diffuse through the Cr_2O_3 layer. The degradation behavior and the integrity of the Cr_2O_3 layer after a long period oxidation in steam environment need to be clarified.

3.3. Methods to improve the oxidation resistance of the Cr coating

The oxidation resistance of the Cr coating in LOCA and beyond LOCA conditions and normal operation conditions is determined by the coating quality, which can be affected by several aspects:

- The compactness, thickness, porosity and integrity of the coatings.

- The chromium grain structures and grain sizes.
- The adhesion strength between the coating and the substrate.
- The heterogeneous particles, oxide inclusions and phase segregation in the coatings.

The oxidation resistance of the Cr coatings is strongly affected by the microstructures and the mechanical properties of the coatings. Several methods can be used to optimize the microstructure and strengthen the mechanical properties of the coatings, including optimization of the fabrication parameters, and optimization of the raw materials and coating pretreatment. In this section, the efforts that the researchers made to improve the oxidation resistance of the Cr coating Zr alloy are reviewed.

3.3.1. Optimization of fabrication methods and parameters

In this part, the researches regarding to the optimization of fabrication parameters of the Cr coating depositing procedure on Zr alloys are introduced. The aim of these works is to achieve better oxidation resistance, stronger adhesion strength, and higher deposition efficiency of Cr coatings.

Although the Cr coatings have been widely used as decorative and functional materials in energy, automotive and aerospace industries, the development of thin Cr coatings for Zr alloy fuel cladding materials in the nuclear industry were started less than ten years ago. Magnetron sputtering [22,37,67,77,78], laser cladding [23], arc ion plating [25,74,79], cold spraying [53,68,80,81] and plasma spraying [24] were reported has been applied for processing Cr coatings on the outside surface of Zr alloy tubes. Moreover, direct liquid injection – metalorganic chemical vapor deposition (DLI-MOCVD), a chemical vapor deposition technology, was successfully used to produce Cr coatings [82] and Cr_xC_y coating [83] on inner surfaces of Zr alloy cladding tubes. PVD and spray methods seem to be the most frequently used methods for Cr coating deposition because of their relatively low processing temperature and minimal oxidation of raw materials. The magnitude of residual stress, grain microstructure and orientation of the coating can be apparently affected by the fabrication methods. Fig. 8 summarizes the EBSD or TEM views of Cr coatings prepared by different methods. All the coatings by PVD methods are constituted of columnar grains elongated along the Normal Direction, and the size of the grains near the Cr-Zr interface is obviously thinner than that near the coating surface. Similar trends concerning about the distribution of grain size were found for cold sprayed Cr coating. Owing to the high velocity impact, the Cr grains appear deformed and elongated, and no vertical columnar grains were observed.

Magnetron sputtering has several advantages: no droplet forming in deposition particle flow, little impurities, high coating uniformity, etc. Although the researchers in Framatome had successfully fabricated full length Cr coated Zr alloy cladding tubes [87], the productivity (namely the deposition rate of coatings) and the formation of columnar crystals are the issues to be solved.

The low deposition rate is one of the drawbacks of magnetron sputtering when using as the coating method for the full-scale cladding tubes. For example, a Cr coating in columnar structure can prepared in a deposition rate of 43.3 nm/min [88], which indicates that nearly 6 h are needed for preparing a 15 μm coating. A very large quantity of the ATF cladding tubes will be demanded due to the wide use of light water reactors around the world. Some efforts should be made to improve the deposition rate of the Cr coating by magnetron sputtering. Up to now, the effective methods include multi-cathodes [89,90], hot target sputtering [77] and melt target sputtering [91,92]. A typical and effective hot target sputtering work was done by the Grudinin et al. [77] They used a hot target high power impulse magnetron sputtering (HiPIMS) system to improve the deposition rate of Cr coatings. By heating the target up to 1200 K, the Cr ions are evaporated during the whole sputtering process, including the DC stage and sputtering stage, which is not good for the compactness of the coating but increases the deposition rate. Besides, the distance between the target and the substrate is less than 100 mm [78]. The temperature of the substrate increased during the sputtering due to the radiation heating from the hot target, resulting in the enhancement of Cr atomic diffusion in the coating layer. The additional heat flux is beneficial for the formation of a denser coating layer, which can improve the oxidation resistance of the coating [93].

The other drawback of magnetron sputtering is the formation of columnar crystals with the same orientation (as shown in Fig. 9), which form a diffusion path for oxygen and weaken the tensile strength of the coating. Chen et al. [94] and Meng et al. [95] studied the effect of bias voltage of the Cr coating structure by using radio frequency magnetron sputtering (RFMS) and direct current

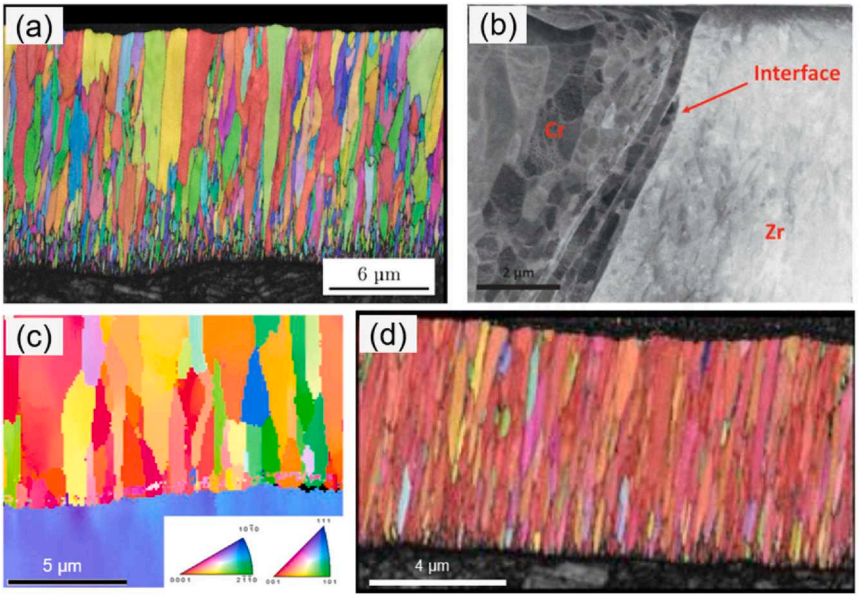

Fig. 8. EBSD or TEM morphologies of the Cr coatings prepared by (a) DC-HiPIMS [84], (b) cold spraying [85], (c) multi-arc ion plating [86], and (d) magnetron sputtering [67]. Reproduced with permission from Ref. [67,84–86].

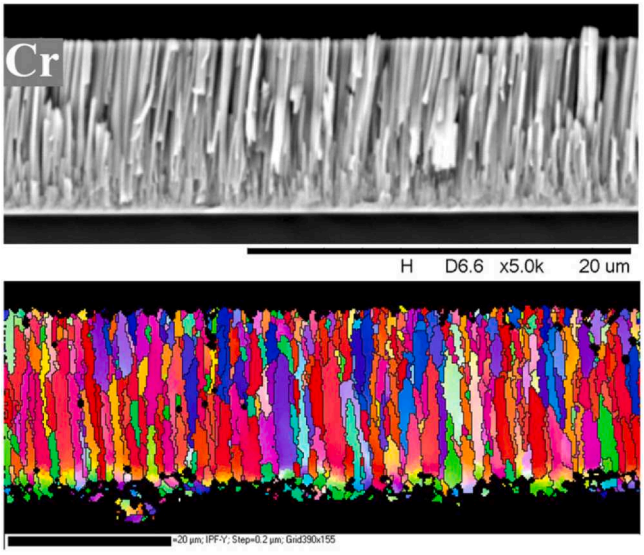

Fig. 9. (a) Cross-section morphology of a typical Cr coating in column crystal structure deposited by hot target high power pulsed magnetron sputtering. (b) EBSD map of a column crystal structure Cr coating - perpendicular Y-direction. Reproduced with permission from Ref. [77] and Ref. [37], respectively.

magnetron sputtering (DCMS), respectively. In the study by Meng et al. [95], the bias voltage, Ar pressure and temperature were changed in turn, and the surface morphologies, the crystal structures and the cross-section morphologies of the as-deposited coatings were observed. The results show that the surfaces present high (110) texture when the parameters presented moderate bias voltage, low Ar pressure and approximately 400 °C. In other words, the coating structure can be controlled by the process parameters. The structure of the coating can apparently affect the oxidation resistance of the coating. A dense 4.5 µm Cr coating and a columnar 9 µm Cr coating were prepared by multi-cathode magnetron sputtering system and hot target magnetron sputtering system, respectively [71]. Then, steam oxidation tests were done in KIT by a thermogravimetry (STA 449, Netzsch). The results show that the activation energy for steam oxidation process of the dense coating and the columnar coating is 202 kJ/mol and 183 kJ/mol, respectively, indicating that the dense one provides a better oxidation resistance. Besides, another feasible method to reduce the proportion of column crystals is HiPIMS. The peak power of HiPIMS can reach 2500 W, which can form a stronger electric field during the sputtering stage and form a denser grain distribution in the Cr coating.

Cold spraying is another frequently applied method for the preparation of Cr coatings. Compared with thermal spray methods (such as plasma spray), the advantages of cold spray are that it can effectively avoid the pre-oxidation of Cr powders, solidification of deposited materials and formation of inclusions in the coatings. The quality of the cold sprayed coating strongly depends on the intrinsic characteristics of the feedstock powder, i.e., the particle size, the shape, and the hardness of the powders. The gas atomization method can produce spherical Cr particles, which has a relatively low hardness and is easy for deformation during the spraying process. Maier et al. [96,97] found that the Cr coating sprayed by gas atomized Cr powders had excellent oxidation resistance in air environment up to 1300 °C. However, the production cost for gas atomized Cr powder is very high because of the high melting point and reactivity of Cr. Moreover, the potential formation of toxic Cr(VI) compounds is not environmental friendly [81]. The method that can obtain Cr powders in a relatively low production cost is mechanical milling of the Cr powders produced by electrolytic reactions, which produced Cr flakes or plates in large sizes. Nevertheless, the inherent residual stresses and limited deformability of the mechanically grinded Cr powder made it hard for the formation of refined grains in the coating [98,99]. In other words, the Cr powders are difficult to compactly bond together, and some cracks may form in the coating, resulting in a poor oxidation resistance of the Cr coatings. Yeom et al. [81] tried to pretreat the mechanically grinded Cr powders by annealing the Cr powders in argon environment at 800 °C for 5 h. It was found that the grain size of the powder increased and the hardness of the powder decreased after annealing, which effectively improved the deformability of the powders and reduced the density of dislocation. Well defined and equiaxed grains were found in the Cr coating produced by the annealed powders, resulting in a relatively strong oxidation resistance of the coating. In summary, the optimization of fabrication parameters for the cold sprayed coating should focus on the quality of the raw materials, namely the grain size, the hardness, the shape and the residual stress of the Cr powders. Additionally, the Cr nano-powder can be tried as raw materials to produce Cr coating by cold spraying in the future.

In addition to magnetron sputtering and cold spraying, some researchers also tried to optimize the fabrication parameters of other coating methods. Kim et al. [23] used the laser beam scanning (LBS) method for the Cr coatings preparation. They found that the surface appearance (including the thickness of the heat affected zone and the homogeneity of the coating) and the ensuing oxidation resistance of the coating was affected by the laser power. Multi-arc plating was performed by He et al. [74] for the Cr coating preparation. The weight gains data of the coated samples after annealing at high temperature showed that the oxidation resistance of the coating was affected by the gas pressures and bias potentials during the coating process. Vacuum arc evaporation method was used by Gautier et al. [100] to fabricate Cr coating, and the effects of Ar pressure, bias voltage and arc current on the texture of the coating were studied. Moreover, a detailed study on the effect of arc current on the microstructure of Cr coatings prepared by multi-arc ion plating was done by Huang et al. [101]. The distribution of grain boundaries, the mean grain size, the crystallographic orientation distribution and the dislocation density of the as deposit Cr coating can be significantly affected by the arc current.

3.3.2. Pretreatment

Pre-annealing thermal treatment is a common method of coating pre-treatment. The purpose of annealing is to facilitate the growth of the initial Cr grains in the coating and thus decrease the density of grain boundaries, which may act as short diffusion paths of oxygen during high temperature steam environment exposure. Researchers from CEA [67] successfully improved the oxidation resistance of magnetron sputtered Cr coating Zr alloys by pre-annealing. In their work, the Cr coated samples with the thickness of about 7 µm was annealed at 700 °C and 800 °C in inert gas environment for 2 h. Then the samples were exposed in steam environment at 1200 °C for 1500 s, and the weight gain rate was compared. Results show that the Cr grain size of the samples increased with increasing temperature after annealing, as shown in Fig. 10. The thermal treatment of coatings may modify the Cr grain boundary atomic arrangement and the atomic transport properties via grain boundaries, thus affect the nucleation of zirconia and the grain boundary diffusion of oxygen and zirconium atoms. Nevertheless, the thermal treatment temperature of the Cr coated Zr alloy should be strictly controlled based on the following three considerations: firstly, the final annealing temperature of the commercially used Zr alloy cladding tubes is about 500 °C [102]. A higher pretreatment temperature of the Cr coated Zr alloy leads the phase transition of the Zr substrate (850 °C), which may affect the mechanical properties and corrosion resistance of the Zr substrate [103]. Secondly, the inter-diffusion between the Cr coating and the Zr substrate would be facilitated by the high temperature, which is one of the main consumption ways of

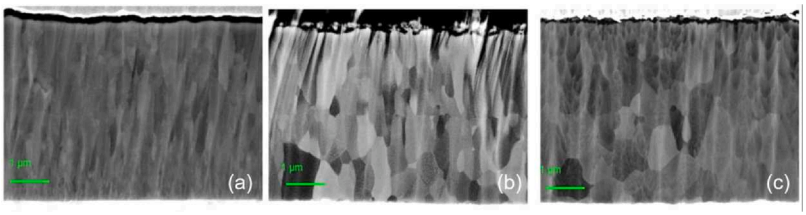

Fig. 10. SEM-BSE morphology of (a) the Cr coating, (b) the Cr coating annealed at 700 °C for two hours, and (c) the Cr coating annealed at 800 °C for two hours. Reproduced with permission from Ref. [67].

Cr coatings [104]. Thirdly, a relatively smaller grain size enhances the tensile strength of the Cr coating [42,105]. Except for directly improving the oxidation resistance, pre-annealing of the coating is benefit for the crack arresting of the coating because of the release of internal stress of the coating and the transformation from columnar grains to equiaxial grains. Vertical cracks are much easier to initiate and penetrate through the parallel grain boundaries of columnar grains under tensile stresses. As for the equiaxial grains, the criss-crossed grain boundaries help to hinder the slips in grains and block vertical crack propagation [86].

The intense pulsed electron beam (Gepulste ElektronStrahl Anlage, GESA) technique is an efficient method for surface modification of materials [106]. Compared to traditional laser surface modification, GESA technique allows the processing of larger surfaces and/or of surfaces with more complex configuration in only one pulse. This method is suitable for the targeted ATF application relies on the chemistry of the applied coating and the hydrothermal stability of the oxide scale that will form in service [107]. Maybe such method can be used to modify the surface of Cr coating in the future.

Laser melting is also a potential method for coating pretreatment, which aims to strengthen the adhesion property and improve the surface density of coatings. For instance, laser melting method is used by Hu et al. [108] on multi-arc ion plated Cr coating Zr alloy samples. The authors found that an interface metallurgical bonding is formed when the laser energy density is high enough to heat the sample surface higher than the Cr-Zr eutectic point. A Cr-Zr fusion zone with a thickness of 60 µm formed after the laser melting process, and the bonding performance of the coating is improved. Nevertheless, the strong diffusion of Cr atoms from the coating into the Zr substrate may affect the oxidation resistance of the coating, which should be further investigated.

For coatings with a relatively high thickness and roughness, cold rolling is an effective method to reduce the coating thickness and enhance the compactness of the coating. Fig. 11 shows the surface and cross-section morphologies of a Cr coated Zr alloy sample before and after cold rolling at room temperature. It can be seen that the thickness of the coating was reduced by 36%, and the uneven outer edges of the as-received sample became uniform after the rolling treatment. However, the cold rolling may cause mechanical damage in the physical structure of the coating. As shown in Fig. 11(a), a crack through the coating and the substrate with a length of nearly 200 µm formed. Moreover, the cold rolling treatment may introduce defects such as dislocations and lead to inhomogeneous local strain distribution. Indeed, the cold rolling is a useful method to compact the coatings produced by spraying or 3D printing. Further works should be done to figure out how to avoid secondary damages on the coatings during the cold rolling process. Besides, how to pre-treat the Cr coated Zr alloy cladding tubes, rather than bulk specimens, by cold rolling should be figured out. Another effective method to reduce the coating thickness is polishing. Polished Cr-cold sprayed coated cladding tubes were prepared and exposed at 1300 °C for 20 min in air by Maier et al. [97] They found the Cr coating was fully intact after the annealing and the thickness of the oxide film was only 5–8 µm.

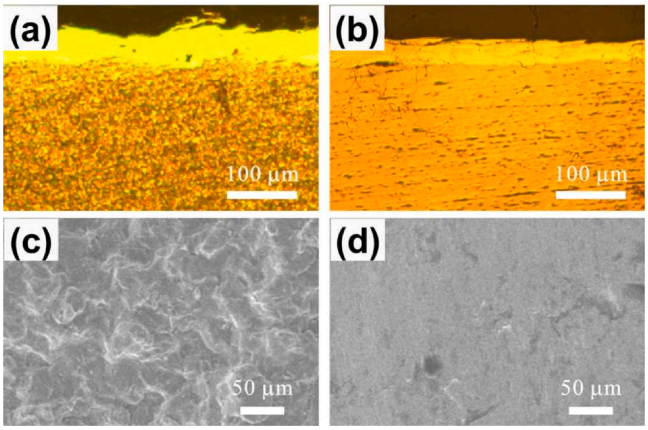

Fig. 11. Surface morphology and cross section morphology of a cold spraying Cr coated Zr alloy sample before and after cold rolling. (a) and (c) are the morphologies before cold rolling. (b) and (d) are the morphologies after cold rolling. Reproduced with permission from Ref. [109].

4. Interdiffusion behavior

The chemical interaction between chromium and zirconium at high temperatures leads to the formation of a Cr-Zr interlayer. In order to improve the neutron economy, the thickness of the coating outside the cladding tubes should be limited as thin as possible. Except for being oxidized, the Cr coating can be considerably consumed by the formation of the Cr-Zr diffusion layer and the inward diffusion into the Zr substrate [104]. Brachet et al. [42] evaluated that the consumption kinetics of the Cr coating by the formation of an oxide film and by diffusion into the substrate in steam environment at 1200 °C are nearly the same. Moreover, the dissolution of chromium atoms into the Zr substrate weakens the strength of the substrate [110]. In this section, the research progress on the Cr-Zr interdiffusion behavior is introduced.

4.1. Structure and chemistry of the Cr-Zr interlayer

4.1.1. As-deposited samples

An interlayer between the Cr coating and the Zr substrate can be formed after the coating preparation procedure. The nano-size structure and chemistry of the interlayer formed on a Cr coated ZIRLO™ cladding material produced by cold spray were studied by Fazi et al. [85] by high resolution transmission electron microscopy (HR-TEM) and atom probe tomography (APT). They found that the intermixed bonding region between the Cr coating and the Zr substrate was a distorted hexagonal close-packed structure (Fig. 12) with a thickness of several nanometers to several tens of nanometers. The layer was formed by an adiabatic shear instability mechanism, which is responsible for the formation of the strong metallurgical bonding due to a highly localized shearing of the substrate and the Cr particles. The 3D reconstruction of APT data showed that the intermixed bonding region contained about

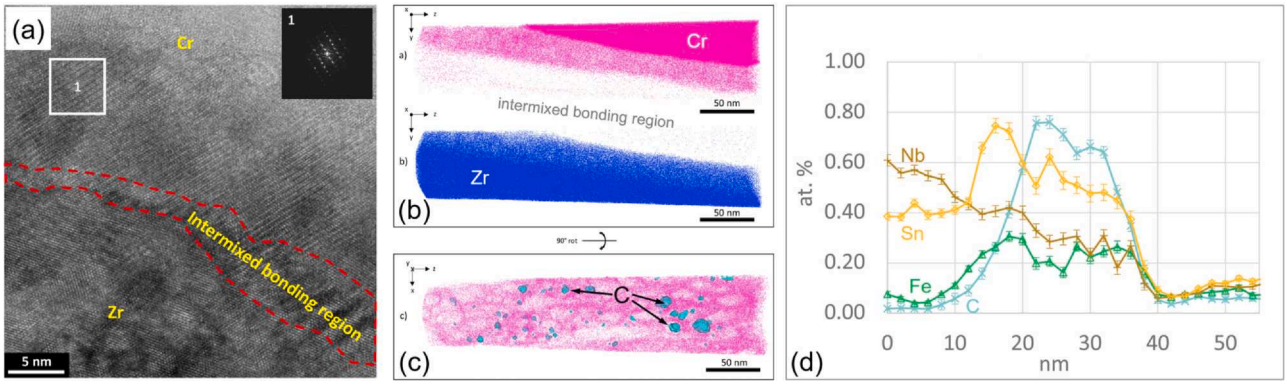

Fig. 12. (a) is the TEM morphology of the Cr-Zr intermixed bonding region (IBR). (b) is the 3D reconstruction of APT data of the interlayer of the Cr coated Zr alloy. The figure shows the distribution of Cr atoms (pink) and Zr atoms (blue) in the IBR. (c) is a 15 nm slice containing the IBR (rotated 90°). The light blue particles in the figure are the carbon impurities. (d) is the EDS result of a scanning line crossing the IBR. Reproduced with permission from Ref. [85].

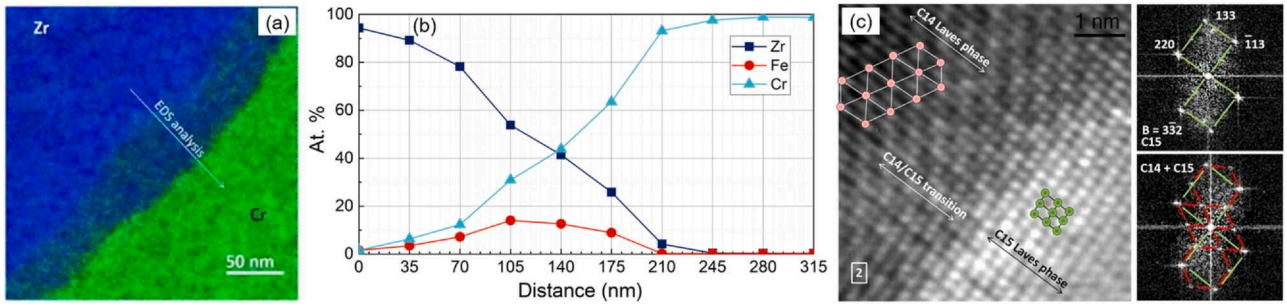

Fig. 13. (a) EDS mapping analysis of the Cr–Zr interface. (b) EDS line scanning of the Cr-Zr interface. The result shows the presence of Fe at the interlayer. (c) TEM analysis of the Cr-Zr interface. C14 and C15 Laves phase is founded. Reproduced with permission from Ref. [113].

60–70 at% Zr, 30–40 at% Cr, 8–10 at% O and 0.80 at% C. The high content of Cr in Zr substrate is due to the significant bulk diffusion of Cr promoted by the localized heat spike that caused by the strong metallurgical bonding during the cold spraying process [111]. Traces of Fe, Sn and Nb were also detected, which are also the alloying elements in the ZIRLO™. The existence of oxygen is due to the residual oxide thin film left on the Zr substrate at the beginning of the coating process, and the detection of carbon in the form of zirconium carbide was owing the residue of grease before the deposition of the coating.

4.1.2. Annealed samples

$ZrCr_2$ is the only intermetallic compound that can be formed in the Zr-Cr system [112]. The $ZrCr_2$ intermetallic compound can be clearly found between the Cr coating and the Zr substrate for the samples after annealing in high temperature environment [25,68,104]. Moreover, a Fe rich zone was observed in the interlayer of a Cr-coated Zircaloy-4 material [113] by TEM-EDS, as shown in Fig. 13.

The enrichment of Fe in the Cr-Zr interlayer is caused by the formation of the $Zr(Cr, Fe)_2$ hexagonal Laves phase (C14) [113,114]. The Laves phases are intermetallic compound phases with AB_2 type structures. They can be classified according to the spatial structure into cubic $MgCu_2$ phase (C15), hexagonal $MgZn_2$ phase (C14) and hexagonal $MgZn_2$ phase (C36) [115]. The content of Fe in the Zry-4 alloy is about 0.2 wt%. At the beginning of the formation of the interlayer, $ZrCr_2$ is formed as a cubic C15 phase. Driven by high temperature, Fe atoms from the Zr matrix diffuse into the $ZrCr_2$ phase, replacing the Cr atoms and resulting in the formation of a $Zr(Cr, Fe)_2$ with a C14 structure. It has been proved that the Fe segregation is able to reduce the interfacial energy of the Cr-Zr system [114]. The Zr $(Cr, Fe)_2$ phase has been found even in Zry-4 alloys without coatings. The formation of $Zr(Cr, Fe)_2$ hexagonal phase (C14) is thermodynamically feasible. The reason why the C14 structural stability is favored by the Fe addition was explained in the perspective of the average electron concentration ratio [113]: the stability of the AB_2 Laves phase is determined by the average electron concentration ratio, namely the ratio of the number of electrons carried by all atoms in the phase to the number of atoms [116]. The C15 structure can exist at a relatively lower average electron concentration, while the C14 structure is stable at a higher average electron concentration. The average electron concentration (e/a) of Fe, Cr and Zr is 8, 6 and 4, respectively. Therefore, after the Fe atom replaces parts of Cr atoms in the $ZrCr_2$ structure, the average electron concentration of the entire Laves phase increases, and thus the transition from the C15 structure to the C14 structure occurs [117].

The formation of $Zr(Cr,Fe)_2$ in the Cr-Zr interlayer can reduce the growth rate of the interlayer. Both Xiang et al. [118] and Nicolai et at. [119] found that the diffusion rate of Cr atoms in $Zr(Cr,Fe)_2$ is five orders of magnitude lower than that in the Zr substrate, which means the existence of the trace $Zr(Cr,Fe)_2$ can effectively restrain the diffusion of Cr from the Cr coating to the Zr substrate. Nevertheless, the content of Fe in Zry-4, M5 and ZIRLO™ (three types of Zr alloys as nuclear reactor cladding tubes) is only about 0.2 wt%, 0.05 wt% and 0.11 wt%, respectively, which is insufficient for the formation of a thick $Zr(Cr,Fe)_2$ layer.

4.2. Growth kinetics of the Cr-Zr interlayer

As already introduced, the consumption rate of the Cr coating by formation of oxide films and by diffusion into the Zr substrate in high temperature environment are of the same order of magnitude

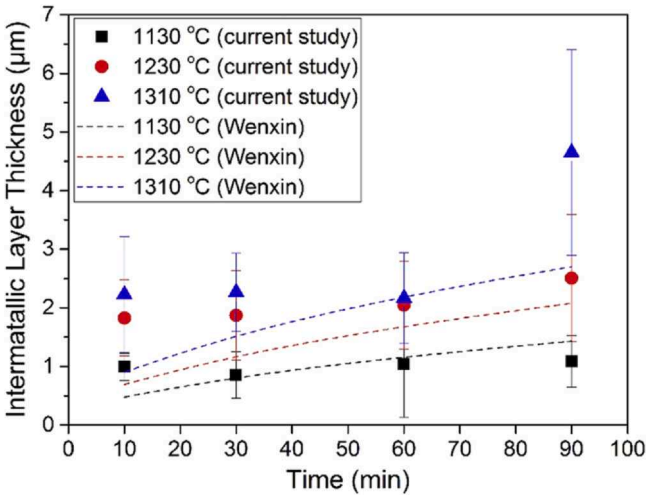

Fig. 14. Growth of the intermediate layer in the Cr coated Zr alloy sample as a function of exposure time and exposure temperature by Yeom et al. The dotted line is the estimated thickness of the interlayer at the same temperature based on the Cr-Zr diffusion couple experiments by Xiang et al. Reproduced with permission from Ref. [68].

at 1200 °C [42]. The growth kinetics of the Cr_2O_3 layer has been studied by many researchers, and some researches also focus on the growth kinetics of the Cr-Zr interlayer.

Xiang et al. [118] used a Cr-Zr diffusion couple to study the growth kinetics of the Cr-Zr interlayer in vacuum environment at 750 °C, 800 °C and 850 °C. Fick's law was used for the mathematical description of the diffusion process in their report:

$$[C(x, t) - C_0] = [C_s - C_0]^*(1 - \mathrm{erf}(x/2\sqrt{D}t)) \quad (7)$$

where C(*x*,*t*) is the concentration of Cr in the Zr matrix; C_0 is the initial concentration of Cr in the Zr matrix (about 0.1 wt%); C_s is the concentration of Cr at the Cr-Zr interlayer when the thermodynamic equilibrium is reached; D is the bulk diffusion coefficient of Cr in β-Zr, which equals to 6.29 $\mu m^2/s$ at 1200 °C [120]. Yeom et al. [68] conducted an experiment on the growth kinetics of the Cr-Zr interlayer of a chromium coated zirconium alloy produced by cold spraying. The experiments were conducted at 1130 °C, 1230 °C, and 1310 °C in steam environment for 10 min, 30 min, 60 min, and 90 min, respectively. The growth of the intermediate layer is shown in Fig. 14. In Fig. 14, the measured thickness of the interlayer at 1310 °C was generally higher than the fitted value, especially for the situation of 90 min: the thickness of the interlayer exceeded 5 μm, which was nearly twice as high as the estimated value. Considering that the standard heat of formation of $ZrCr_2$ and Cr_2O_3 is −256 kJ/mol and −1128 kJ/mol, respectively, the researchers speculated that the mismatch is due to the heat release of the oxidation process. Therefore, the actual temperature of the specimen was higher than the target temperature, accelerating the diffusion rate of both Cr atoms and Zr atoms.

In order to avoid the interference of heat release from oxidation reaction on the diffusion kinetics evaluation, Yang et al. [104] conducted a series of Cr-Zr interaction experiments in inert gas environment. Magnetron sputtered and cold sprayed Cr coating on Zr alloy specimens were used as samples for annealing tests at a temperature range from 1100 °C to 1300 °C. They concluded that the diffusion process can be divided into two stages. At the early stage, the Zr-Cr inter-diffusion is a reaction-diffusion process. $ZrCr_2$ was formed by the chemical reactions between Cr and Zr atoms, and the growth of interlayer was controlled by the reaction rate. The formation rate of the $ZrCr_2$ layer at the beginning is relatively high because of the absence of a diffusion barrier. Then, after the initial $ZrCr_2$ layer formed, the growth of the interlayer became diffusion controlled. The global inter-diffusion coefficient gradually decreases with the growth of the Cr-Zr interlayer. Fig. 15 shows the evolution of the Cr-Zr interlayer thickness as a function of exposure time at 1300 °C in inert gas environment. It is worth to note that the thickness of the interlayer began to decrease after 2 h annealing, which is due to the dissolution of Cr atoms into the Zr substrate. The solubility of Cr in β-Zr is up to 8 at% at 1300 °C [121]. In consequence, a considerable amount of Cr atoms from both the Cr coating and the Cr-Zr interlayer diffused into the Zr solid solution, resulting in the disappearance of the residual Cr coating and the interlayer after long-term exposure in high temperature environment.

Table 2 summarizes the thickness of Cr-Zr interlayer in Cr coated Zr alloy samples in steam environment at different temperature. The thickness data was measured based on the figures given in the reference paper. The preparation method of the Cr coating can affect the growth rate of the Cr-Zr interlayer. For instance, the growth rate of the interlayer in the cold sprayed samples is slightly higher than that in the magnetron sputtered samples in the study [104]. They inferred that the difference in the atoms diffusion rate was caused by the residual oxide film between the Cr coating and Zr substrate: the ballistic cleaning effect of the cold spray process can effectively remove the residual ZrO_2 thin layer on Zr substrate. After the spraying process, Cr powder particles at the interface are embedded in the original surface of the Zr substrate [122]. As for the magnetron sputtering, although an etching process is usually performed before sputtering, the relatively lower deposition speed can hardly clean the substrate surface. For example, carbon in the form of zirconium carbide was detected in the intermetallic layer of a Cr coating Zr alloy, which is owing the residue of grease before the deposition of the coating [85].

The objective of the ATF cladding materials is to offer additional coping time under severe accident conditions. As for the Cr coated

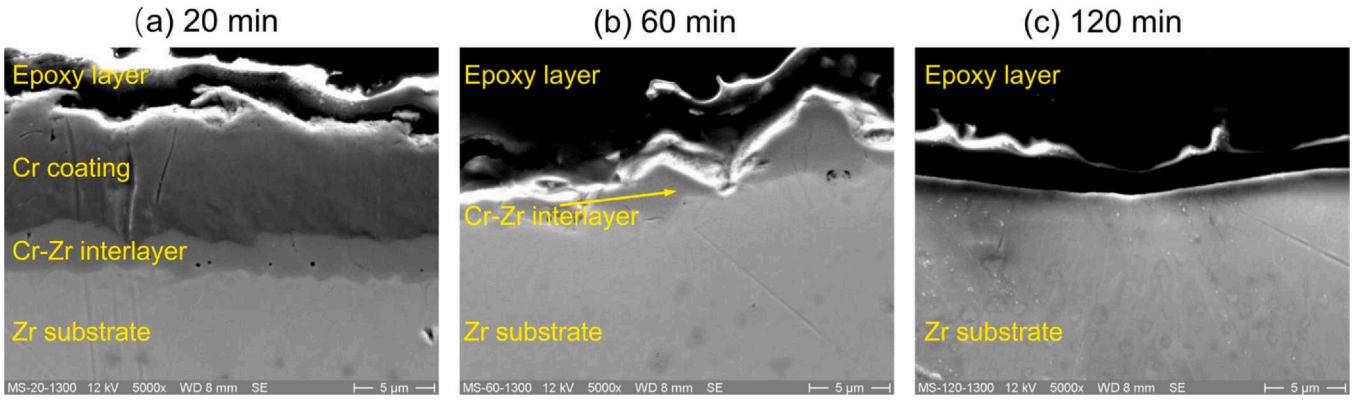

Fig. 15. Evolution of the Cr-Zr interlayer thickness as a function of exposing time at 1300 °C in inert gas environment. Reproduced with permission from Ref. [104].

Table 2
Summary of the thickness of Cr-Zr interlayer from literatures.

Date source	Coating method	Exposure temperature (°C)	Exposure time (min)	Measured value (μm)
Fig. 12(b) from Ref. [42]	Magnetron sputtering	1200	5	0.62
Fig. 6(b) from Ref. [67]	Magnetron sputtering	1200	5	0.55
Fig. 7(a) from Ref. [72]	Magnetron sputtering	1100	30	0.76
Fig. 3(h) from Ref. [74]	Multi arc ion coating	1060	60	0.51
Fig. 5(a) from Ref. [68]	Cold spray	1310	90	4.62
Fig. 8(c) from Ref. [25]	Vacuum arc plasma spray	1200	60	4.09
Fig. 5(a) from Ref. [24]	Air plasma spray	1200	60	2.95

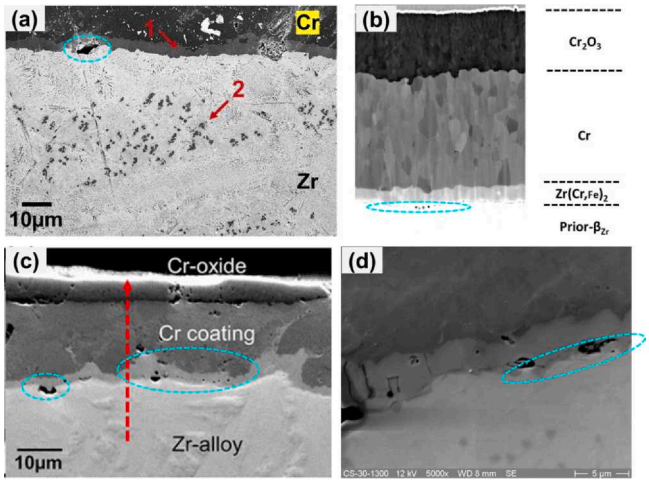

Fig. 16. Cavities between the Cr-Zr interlayer and the Zr substrate. Reproduced with permission from Ref. [67,68,96,104].

Zr alloy, increasing the "survival time" of a coating is beneficial for prolonging the coping time under severe accident conditions. The oxidation kinetics is widely used for the evaluation of the lifespan of a coating in high temperature steam environment, but this method is inaccurate because the coating can lose its protectiveness even the residual coating remains (the degradation mechanism has been introduced in the Section 1.2.2). Moreover, the diffusion kinetics is also used to estimate the lifespan of the Cr coated Zr alloys. Yang et al. [104] used a modified parabolic law to estimate the consumption of the Cr coating as a combined result of the formation of the Cr-Zr interlayer and the dissolution of Cr atoms in the Zr substrate. A preliminary model of the overall Cr coating consumption by Cr_2O_3 formation and Cr dissolution under LOCA conditions was derived by Brachet et al. [42] This model is useful for the evaluation of the lifespan of the Cr coating. Further studies should focus on how the combined degradation mechanism by oxidation and diffusion affect the evaluation model. Indeed, the coping time is hard to estimate by modeling. Experiments under prototypical conditions (temperatures, heating rates, inner pressure) are needed for the estimation.

4.3. Diffusion related phenomena

In this section, the special structures formed in the Cr coated Zr alloys due to the diffusion of Cr, Zr and other metallic atoms are introduced.

First, cavities are formed between the Cr-Zr interlayer and the Zr substrate in the Cr coated Zr alloys after annealing at high temperature. This kind of cavities have been observed by many researches, as shown in Fig. 16. The widely accepted explanation for the formation mechanism of the cavities is based on the Kirkendall-type effect, which refers to the movement of diffusion interface due to the difference of relative diffusion coefficients of the atoms [123]. The activation energy of the diffusion of Cr atoms in zirconium is about 134–160 kJ/mol, while the activation energy of the Zr atoms in chromium is about 366 kJ/mol [124]. Moreover, the solubility of Cr in β-Zr is much higher than that of Zr in chromium. These two differences contribute to the larger inward diffusion flux of Cr atoms within the Zr substrate than the outward diffusion flux of Zr atoms within the Cr coating. Therefore, a back diffusion flux of vacancies from the Zr substrate is induced by the dissymmetric atomic diffusion at the interface between the Cr-Zr interlayer and the Zr substrate. Finally, clustering and coalescence of Kirkendall vacancies lead to the nucleation and growth of the cavities. Liu et al. [125] suggested that it is the larger elemental outward diffusion flux (including Zr, Fe, and Sn) lead to the formation of these cavities based on the fact that cavities distributed inside the Zircaloy substrate and close to the $ZrCr_2$/Zircaloy interface and the theory of Kirkendall effect that Kirkendall cavities invariably formed at the side of the metal whose diffusion coefficient is larger. However, the larger elemental outward diffusion flux is contrary to the diffusion and solubility data between Zr and Cr mentioned above. Therefore, the authors suggested that it is the formation of α-Zr(O) and $ZrCr_2$ phases inhibit the inward diffusion of Cr at the later oxidation stage and finally resulted in the peculiar distribution of cavities. The sizes of the cavities are related to the exposure time and temperature. For instance, the diameter of the cavities formed on a Cr-coated Zr alloy sample after exposure in steam environment at 1200 °C for 300 s is about tens of nanometers [67] (Fig. 16(b)), and the size of the cavities on a sample after 30 min exposure at 1300 °C significantly increased to about 10 μm [104] (Fig. 16(d)). Up to now, the effect of the cavities on the mechanical properties and the oxidation/diffusion resistance of the coating is still unknown. The existence of the cavities under the Cr-Zr interlayer should be considered in further studies, especially for simulation studies of the mechanical behavior of the Cr coated Zr alloys.

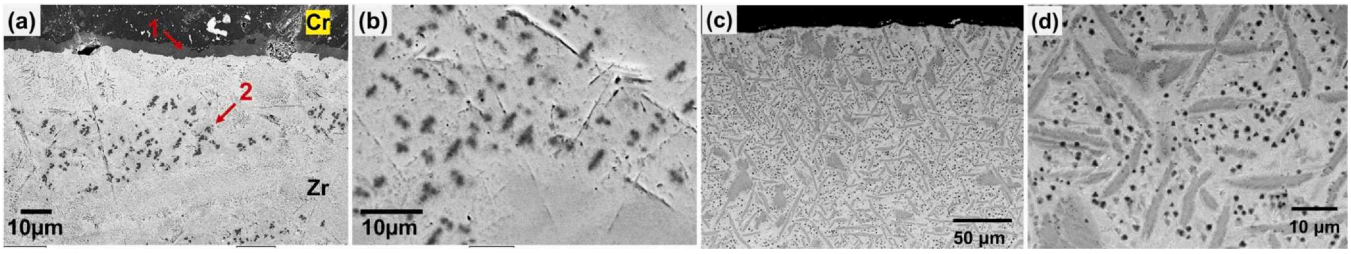

Fig. 17. The morphology of the black dots formed in the Zr substrate under the Zr-Cr interlayer. Reproduced with permission from Ref. [68,104].

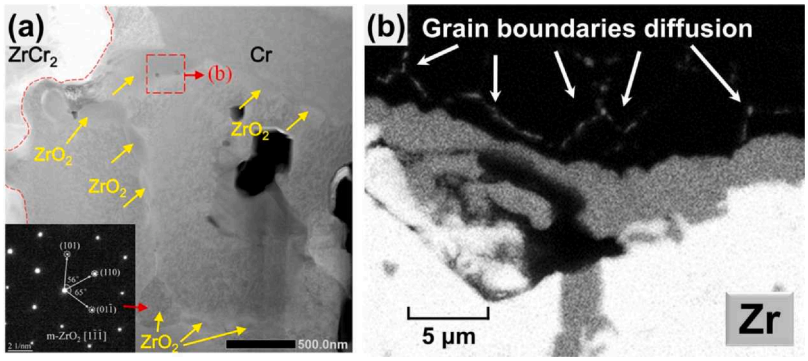

Fig. 18. Proofs for the grain boundaries diffusion of Zr in the Cr coating observed by (a) TEM and (b) SEM. Reproduced with permission from Ref. [104,125].

Second, alloy precipitates in the bulk alloys are observed. After the exposure in high temperature steam environment, some dots formed in the Zr substrate beneath the Cr-Zr interlayer. The color of the dots is black when observed by SEM, while white by optical microscopy (OM). Fig. 17 shows the morphologies of some dots observed by SEM from different literatures. It has been confirmed that the black dots are $ZrCr_2$ precipitates according to EDS scanning results [24,37]. The formation of the $ZrCr_2$ precipitates is due to the different solubilities of chromium in α-Zr and β-Zr. The solubility of Cr in β-Zr at 1200 °C is about 2.5%–3% (atom percent) [7,126], and it can reach to about 8% at 1300 °C [68]. The phase transition of α-Zr to β-Zr is completed at 910 °C, which means that the Zr substrate is in the β phase under LOCA conditions. Therefore, large amounts of Cr from the coating diffused and dissolved into the Zr substrate under LOCA conditions. During cooling, the lower solubility of Cr in α-Zr results in the formation of $ZrCr_2$ precipitates in the Zr substrate. As shown in Fig. 17(d), the $ZrCr_2$ precipitates are mainly inside the laths of Widmanstätten structures. Zr atoms can also spread into the Cr coating layer. As already introduced in the Section 1.2.2, Zr atoms from the Zr substrate diffused outward along the Cr grain boundaries and reacted with the inward diffusing oxygen. Fig. 18 is some proofs for the grain boundaries diffusion of Zr in the Cr coating observed by SEM [104] and TEM [125]. It can be seen that Zr atoms gathered at the Cr grain boundaries. A distinct accumulation of Zr atoms at the beginning of the diffusion path was found, which is due to the limited diffusivity and solubility of Zr in chromium [67].

Third, Sn-containing precipitates inside the Cr_2O_3 scale are observed. During the steam oxidation of Cr-coated Zr alloy at high temperature, not only Fe and Zr in substrate can diffuse outward to the Cr coating, but the outward diffusion of Sn was also observed by Liu et al. [125] This outward diffused Sn precipitated on the grain boundaries of Cr_2O_3 and inside the Cr_2O_3 grains during the oxidation of Cr coating. Fig. 19 shows the morphologies of the Sn-containing precipitates inside the coating. The further Kirkendall effect of these Sn-containing precipitates leads to the formation of microcavities inside the Cr_2O_3 scale and affects the microstructural integrity of the Cr_2O_3 scale. The effect of the outward of Sn and the following behavior of Sn inside the coating on the oxidation behavior of the Cr-coated Zircaloy need to be further investigated.

4.4. Diffusion barrier

As discussed above, the interdiffusion between the Cr coating and the Zr substrate is a critical issue for the applying of Cr coated Zr alloys as ATF cladding material. Firstly, the dissolution of Cr atoms in the Zr substrate consumed parts of the Cr coating, resulting in the reduction of the survival time of the coating. Secondly, the Kirkendall cavities formed between the Cr-Zr interlayer and the Zr substrate may affect the mechanical properties of the coating, resulting in cracks or blisters in the coating. Thirdly, the dissolution of Cr into the Zr substrate may increase the brittle thermo-shock behavior during the re-injection of coolant process. Fourthly, the Cr-Zr eutectic temperature is about 1332 °C. if a beyond design basis accident happens, the Cr-Zr eutectic reaction would occur and the protectiveness of the coating would totally disappear. Fifthly, the outward diffusion of Zr along the Cr grain boundaries enlarges the diffusion paths of oxygen, resulting in the loss of protectiveness of the Cr coating and the ensuing breakaway oxidation of the Zr substrate. The simplest way to restrain the interdiffusion between the Cr coating and the Zr substrate is to add a diffusion barrier between the Cr coating and the Zr substrate.

Michau et al. from CEA [127] made an additional thin Mo layer between the Cr layer and the Zr substrate. The oxidation test result of the new Cr-Mo coated Zr alloy in air at 1100 °C showed that the consumption rate of the residual Cr coating of the Cr-Mo coated sample was lower than that of the pure Cr coated sample. The

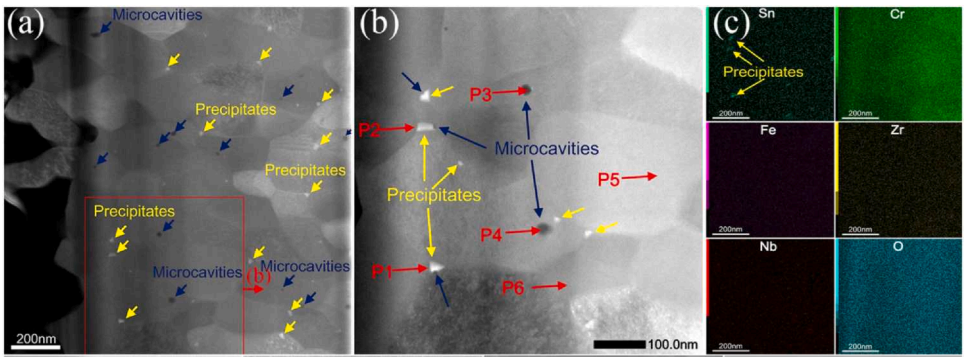

Fig. 19. TEM characterization of the Cr_2O_3 layer on a Cr coated Sn containing Zircaloy after annealing in steam environment for 1 h: (a) Scanning TEM micrograph of Cr_2O_3 layer in low magnification; (b) Scanning TEM micrograph of Cr_2O_3 layer in high magnification; (c) EDS mapping results of (b). Reproduced with permission from Ref. [125].

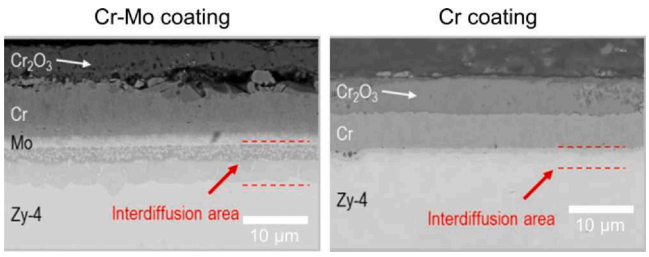

Fig. 20. Cross section morphology of the Cr-Mo coated Zr alloy sample after annealing in air at 1100 °C for 60 min. The Mo-Zr interdiffusion area is obviously larger than the Cr-Zr interdiffusion area.

amounts and growth rate of the Kirkendall holes also decreased in the Cr-Mo coated sample. The Mo layer obviously delayed the Cr-Zr eutectic reaction under B-DBA conditions. However, a Mo-Zr interlayer with a thickness higher than the Cr-Zr interlayer formed after 60 min exposure (Fig. 20). The fast inter-diffusion behavior between Zr and Mo [128] should be considered for the design of diffusion barrier.

A CrN/Cr multilayer coating was prepared by Sidelev et al. [129] to enhance the oxidation resistance and restrain the interdiffusion behavior. The results show that the weight gain of the multilayer coated specimen decreased by almost half compared with the pure Cr coated specimen after being annealing in air at 1100 °C. CrN decomposed into Cr_2N and N_2, and the inward diffusion of N_2 resulted in the formation of ZrN, which can prevent Cr diffusion into the Zr substrate.

Moreover, Wang et al. [130] prepared a ZrO_2/Cr bilayer coating on Zr alloy. The ZrO_2 layer and the Cr layer was deposited by plasma electrolytic oxidation and filtered cathodic vacuum arc deposition, respectively. The researchers found that the addition of ZrO_2 can reduce the weight gain rate of the Zr alloy specimen, compared with pure Cr coated Zr alloy specimen, which is due to the ZrO_2 layer suppresses the inward diffusion of oxygen and the outward diffusion of Zr. In high temperature condition, the ZrO_2 layer decomposes into Zr_3O and α-Zr(O), forming an α-Zr(O) layer and a Zr_3O layer. However, the dissolution of the ZrO_2 layer may embrittle the Zr substrate, which is an issue of this type of coating that to be solved.

5. Mechanical behavior

Compared with ceramics coatings, the metallic Cr coatings exhibit higher tensile strength because of the relatively higher ductility and fracture toughness [131]. In the real reactor environment, the cladding tube is subjected to two orientation of mechanical loadings, i.e. along its axial and circumferential directions [132]. The mechanical behavior of the Cr coated Zr alloy cladding tubes under LOCA conditions is apparently affected by the stress state of the cladding tubes, which is determined by the formation of fission gases in the cladding tubes, the interaction between the fuel pellets and the cladding tubes, and the pressure of the coolant water outside the tubes[45]. Cracks may appear in the coating due to the tensile stress, resulting in acceleration of oxygen diffusion along the cracks and the ensuing accelerated oxidation of the coating under LOCA conditions. In this section, the studies regarding the mechanical behavior of the Cr coated Zr alloys cladding materials in normal operation conditions and accident conditions are reviewed. Some researches on strength assessment, cracks evolution and fracture mechanisms were done at room temperature because the microcosmic observation and stress analysis is hard to perform at the extreme high temperature under LOCA conditions.

5.1. Crack formation and crack growth

The formation of cracks in the Cr coating can lead to the loss of protectiveness of the coating in a very short time because of the fast diffusion of oxygen along the cracks. Once the oxygen ions reach the Zr substrate, the volume expansion of the Zr substrate due to the newly formed ZrO_2 results in growth stress in the coatings. The fracture mechanism of the coating under high temperature steam environment is a coupled mechanism involving oxidation reactions and tensile stress. Up to now, only few tensile tests and in-situ observation of the coated cladding tubes were done in high temperature steam environment. However, the surface crack evolution is crucial for understanding the fracture mechanism of the Cr coated Zr alloys under LOCA conditions.

Tensile tests and three-point bending tests on Cr coated Zr alloy specimens were done by Jiang et al. [133,134] to investigate the initial location and the propagation behavior of the cracks in the Cr coating. Most of the cracks initially formed at the interface of the coating and the substrate (Fig. 21(a)), followed by vertical propagation of the cracks to the coating surface (Fig. 21(b)) with the increasing of tensile strains. In other words, the local tensile stress in the interface zone is the largest during the tensile test, which has been proved by finite element (FE) analysis [133]. These vertical cracks can easily penetrate along the grain boundaries of the Cr coating to form surface cracks because of the columnar crystal structure of the magnetron sputtered coating [37]. Also, some cracks initiated from the micro-defects zone at the surface of the coating. A model of Cr coated Zr alloy with an initial oblique crack in the coating was created by Xu et al. [135] to investigate the crack length, coating thickness, initial crack inclination angle on the crack propagation behavior. They found that the crack propagation in the

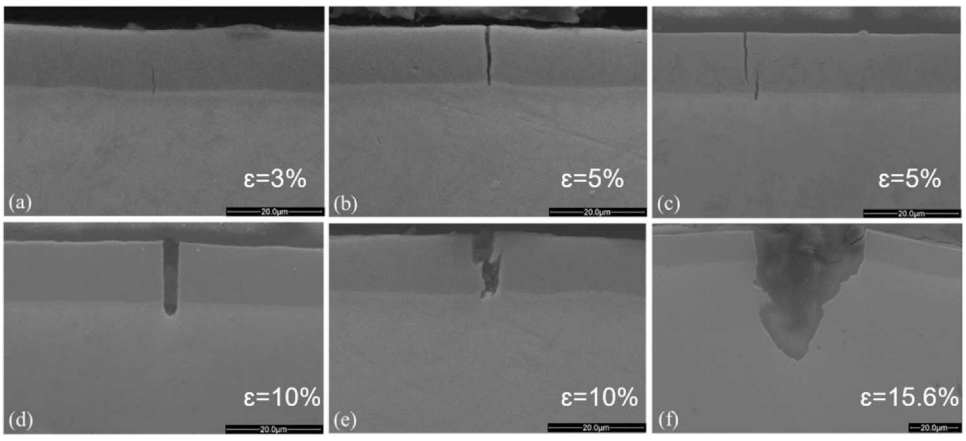

Fig. 21. Crack initiation and propagation in a Cr coating at different tensile strains. Reproduced with permission from Ref. [133].

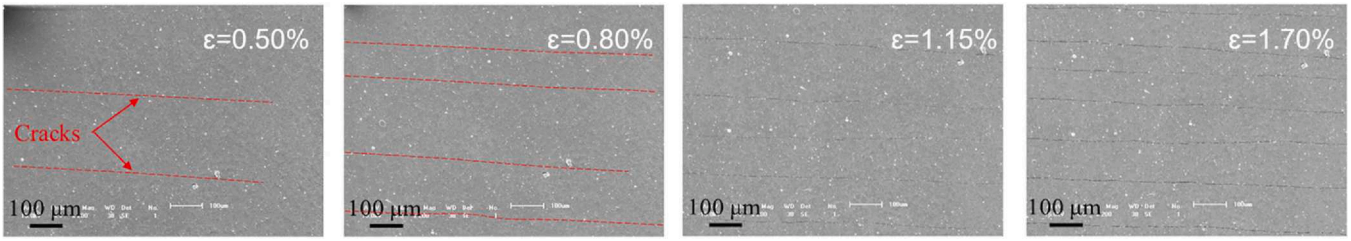

Fig. 22. Surface crack evolution of a Cr coated Zr alloy sample under different tensile strains at room temperature. Reproduced with permission from Ref. [131].

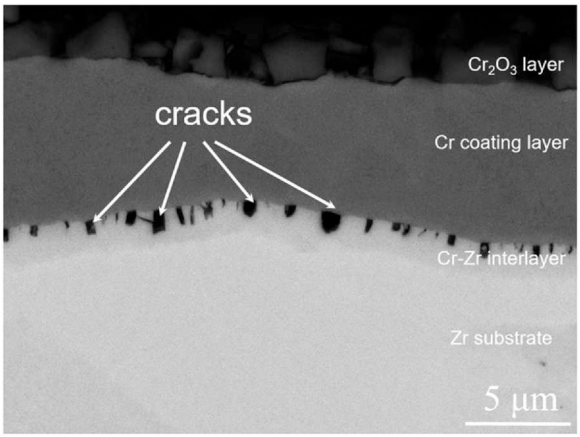

Fig. 23. Cross section morphology of the Cr coated Zr alloy specimen after pre-oxidizing in steam environment at 1000 °C for 1 h and tensile testing. Cracks can be found at the Cr-Zr interlayer zone. Reproduced with permission from Ref. [86].

plane vertical to the axial direction is controlled by the opening mode crack. The type of coating failure owing to the crack propagation varies with the change of initial crack inclination angle and initial crack length. Based on the in-situ observation of the morphologies of the coating surface during the tensile test, Jiang et al. [131] found that the Cr coating exhibited brittle and ductile cracking behavior at room temperature and 400 °C, respectively. The duration to failure of the coating and the deformation compatibility between the coating and the substrate is better at 400 °C compared with those at room temperature [105,136]. Further studies should be done at typical accident temperatures to figure out the tensile performance of the Cr coated Zr alloy cladding tubes.

Expanding plug tests were performed in room temperature on Cr coated Zr alloys by Roache et al.[137] During the tests, spatial strain maps and acoustic energy evolution were correlated by in situ 3D-DIC and AE monitoring. For the expanding plug tests, cracks initially formed at 0.40% ε_{hoop}, and the direction of the cracks is axially around the circumference of the tube sample.

The impact of steam should be considered for discussion of the fracture mechanism of the cladding tubes during tensile tests. Fig. 22 shows the surface crack evolution of a Cr coated Zr alloy sample under different tensile strains at room temperature. It can be seen that the cracks parallelly formed one by one before the completely fracture. Indeed, the real fracture process of Cr coated tubes under LOCA conditions should be different with the process in Fig. 22 because that the high temperature conditions and oxidation behavior can affect the mechanical behavior of the coating. Up to now, only the effect of high temperature on the cracks initiation and propagation is studied. A series of tensile tests and three-point bending tests were done on pre-oxidized Cr coated Zr alloy samples by Jiang et al. [86,138] They found that cracks are easily initiated at the newly formed brittle Cr-Zr interlayer ($ZrCr_2$ phase). As can be seen in Fig. 23, many transgranular cracks are formed in the Cr-Zr interlayer. The cracks are all blocked in the interlayer other than penetrating to the Cr coating or the Zr substrate, indicating that the fracture toughness of the Cr-Zr interlayer is lower than that of the other parts of the Cr coated Zr alloys. Further studies should consider the impact of coating/substrate oxidation on the mechanical behavior of the coating. In LOCA conditions, oxygen can easily penetrate into the coating along the crevice in the coating once the surface cracks formed. Then, the formation of ZrO_2 leads to the increase of growth stress on the coatings because of the friability of ZrO_2. In this case, just one crack is enough for the total fracture of the whole cladding tube. Moreover, whether the stress can affect the diffusion of oxygen ions along the grain boundaries in the Cr coating is unknown, which should be figured out in the future.

5.2. Effect of the coating on the mechanical property of the cladding tubes

The existence of Cr coating on the Zr alloy surface can affect the mechanical properties of the cladding tube, which can be judged by the adhesion properties, the burst resistance and the hardness trend of the Cr coated Zr alloy cladding tube. Several studies have been done on this topic.

The adhesion property is a key issue for surface coatings. Due to the harsh environment in accident condition, i.e., thermal expansion, drastic oxidation, irradiation growth and ballooning, the severe deformation of the cladding tube may cause the coating peeling off from the Zr substrate. Ring tensile and compression tests were done by several research groups [44,47,139] to evaluate the adhesion properties and the strength of the Cr coating. As shown in Fig. 24, the tensile strength and the compressive strength of the Cr coated Zr alloy ring sample (prepared by 3D laser coating) is slightly higher than that of the uncoated sample, and the variation trend of stress-strain curves basically remain the same. No peeling or spalling phenomena were found on both the tensile sample and the compression sample. The tensile test of dog-bone shape Cr coated Zr alloy samples performed by Jiang et al. [86] also indicates that the strength and elongation of the samples are significantly improved by the coating. Červenka et al. [139] found that the Cr coated specimens feature a significantly longer time to underdo the ductile-brittle transition. The improvement of the strength of the coated samples is due to the relatively higher hardness of the Cr coating: microhardness measurement results of the as-deposited [44] and the oxidized [53] (normal operation conditions) Cr coated Zr alloy shows that the hardness of Cr coating is higher than that of the Zr substrate. However, it is notable that the relation of the hardness between the coating and the substrate can be different during accident scenario because of the change of the crystal structures and grain sizes [68]. Indeed, the stress relaxation and grain coarsening after a high temperature annealing process leads to the change of strength of the Cr coating. As for the Zr substrate: the uncoated Zr alloy nearly completely loses it strength at temperatures when the α to β phase transformation occurs, which results in strong ballooning and burst of the tubes. The existence of the Cr coating reduces this effect due to hardening of the Zr by Cr diffused into the bulk.

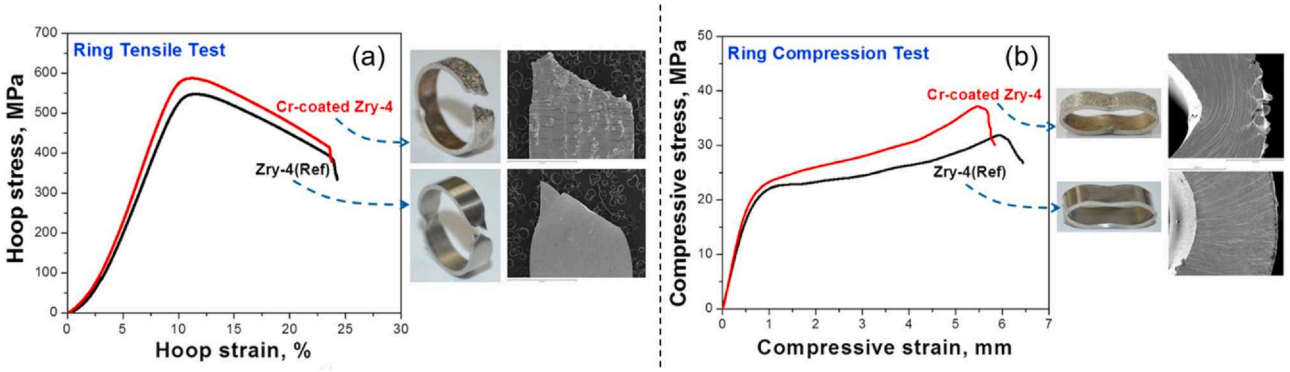

Fig. 24. (a) Ring tensile test results and the picture of the Cr-coated Zr alloy ring after the tensile test. (b) Ring compression test results and the photographs of the Cr-coated Zr alloy ring after the compression test. Reproduced with permission from Ref. [44].

The ballooning and rupture behavior of a cladding tube is crucial to the fuel stability in LOCA and beyond LOCA conditions. Owing to the temperature increase and core pressure decline in LOCA conditions [140–142], ballooning and rupture of the cladding tubes usually occur. The burst resistance of the cladding tubes can be improved by the existence of the Cr coating. Park et al. [109] performed burst tests of the Cr coated Zr alloy tube samples in simulated LOCA conditions to investigate the ballooning behavior. As shown in Fig. 25, the burst temperature of the coated sample is higher than that of the uncoated sample, and the burst opening of the coated sample is much smaller than that of the uncoated one. Moreover, no significant peeling or spalling phenomena was found after the integral LOCA test. Similar tests were done by Kim et al. [44]: partially Cr-coated Zr alloy tubes were used to perform the LOCA simulated ballooning test. It can be clearly seen that the cladding rapture is located at the uncoated region of the tube. The improvement of the burst resistance of the coated cladding tubes is owing to the increasing thickness of the whole cladding tubes and the improved strength of the Cr coating. A recently published study by Hazan et al. [143] reported comparison results of semi-integral LOCA test of cold sprayed Cr coated Zr alloys and bare Zr alloys. The Cr coated Zr alloy tube underwent burst after 30 min with maximal hoop deformation of 14.5%, while the uncoated Zr alloy tube underwent burst after 350 s with maximal hoop deformation of 178%. The authors speculated that the relatively lower creep rate of Cr compared with Zry-4 at 800–900 °C is the reason for the lower ballooning behavior of the coated tube. Additionally, creep tests of the coated and uncoated Zr alloys at 750 °C and 850 °C were performed by the researchers from CEA [144]. Similar results regarding to the size of the burst opening, the coating adherent, and the duration time were obtained.

The fatigue behavior of alloys is used for the evaluation of the strength of alloys. Fatigue tests of Cr coated Zr alloys were done by Ma et al. [145] Remarkable plastic deformation was found in the Cr coating with the Zr substrate, indicating high fracture toughness and good ductility of Cr coated Zr alloy is high. Moreover, in-situ observation of the coating during the fatigue test shows that no crack initiation is found until the late stage of fatigue life. In a word, the fatigue life of the Zr alloy is improved by the Cr coating.

The hardness of claddings can be improved by the Cr coating. For instance, the hardness of a cold sprayed Cr coating ZIRLO™ cladding and a bare ZIRLO™ cladding is 392 ± 52 and 261 ± 26 HV, respectively [146]. As a result, the wear resistance of the Cr coated cladding is improved by 80–90% compared with the uncoated cladding, which is obtained by fretting wear tests in simulative Grid-to-Rod-Fretting (GTRF) environment by Reed et al. [146].

6. Failure mechanism

Although the Cr coating can prolong the survival time of the Zr alloy in DBA and beyond BDBA conditions, some external or internal parameters of the coating may result in the breakaway oxidation of the cladding in a short time. In this section, the failure mechanisms of the Cr coating induced by different parameters are discussed.

6.1. Cr-Zr eutectic

According to a safety guide by IAEA, the frequency of occurrence of design basis accidents and beyond design basis accidents is 10^{-4}–10^{-2} and 10^{-6}–10^{-4} per reactor year, respectively [147]. The melting point of chromium and zirconium is 1907 °C and 1855 °C, respectively [148,149], but the Cr-Zr eutectic temperature is 1332 °C, which

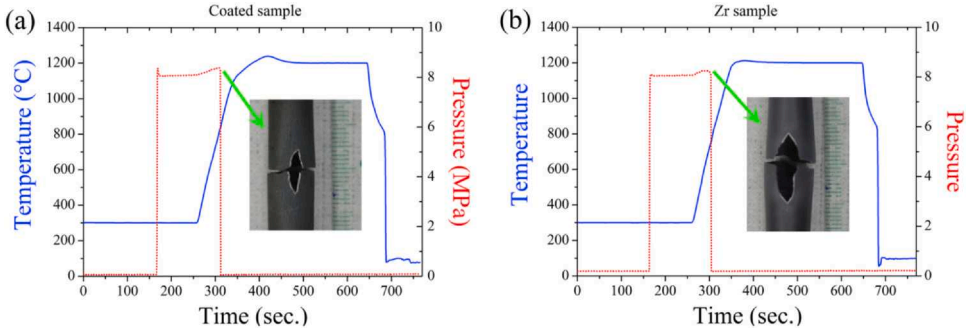

Fig. 25. Comparation of the explosion pressure and temperature between the (a) Cr coated Zr alloy cladding tube and Zr alloy cladding tube under simulated LOCA conditions. The photographs of the burst openings are shown in the embedded figures. Reproduced with permission from Ref. [109].

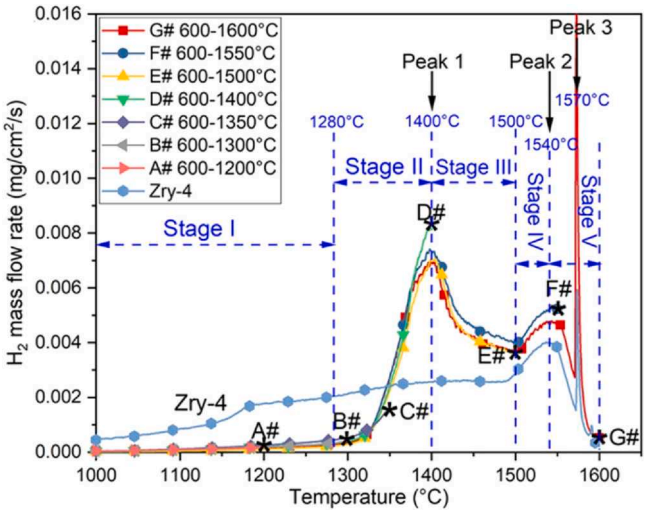

Fig. 26. Temperature profile and hydrogen flow rates of a series of transient test of a Cr coated Zr alloy sample in steam environment from 1000 °C to 1600 °C. Three sharp increases of hydrogen release were observed. Reproduced with permission from Ref. [151].

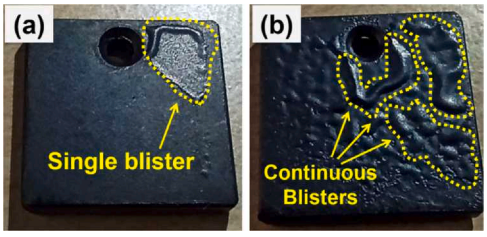

Fig. 27. The macro morphology of Cr coated Zr alloy after the steam oxidation test at 1400 °C for 5 min. Some blisters formed on the samples surface.

is higher than the typical core temperature during a design basis accident (maximal 1200 °C). If a beyond design basis accident happens, the core temperature may rise beyond the Cr-Zr eutectic temperature. The Cr coating that connects with the Zr substrate would melt in a short time, resulting in the formation of a eutectic liquid interlayer.

The metallurgical evolutions of the Cr coating Zr alloy beyond 1300 °C were analyzed, e.g. by the researchers from KIT [150], CEA [67] and CTU Prague [37,110]:

Stage 1: During temperature rise to 1332 °C, the phase transfer of zirconium from α-Zr to β-Zr and the formation of $ZrCr_2$ intermetallic phase occur.
Stage 2: At temperatures higher than 1332 °C, the Cr-Zr eutectic reaction occurred at two places: one is the interlayer between the $ZrCr_2$ and the β-Zr, and the other is inside the Zr-substrate owing to the inward diffusion and dissolution of Cr from the coating. Due to the capillary effect of potential liquid, the newly formed eutectic products gathered at some active sites in the Zr substrate. Finally, the Cr coating was totally consumed and lost its protectiveness. At the same time, the fast-diffusing Zr in liquid phase reacts with the Cr_2O_3 layer to form ZrO_2 and Cr, and the newly formed Cr rapidly melts with Zr, resulting in a certain oxygen flow through the Cr_2O_3 layer. In summary, the dense structure of Cr_2O_3 layer can be destroyed by the Cr-Zr eutectic reaction, the reduction reaction of Cr_2O_3 by Zr atoms that diffuse from the Zr substrate, and the volatilization of Cr_2O_3. As a result, O_2 and H_2O molecule rapidly diffused into the Zr substrate, leading to in the accelerated oxidation of the Cr coated Zr alloys. The Cr-Zr eutectic reaction takes place rapidly at the temperature above the Cr-Zr eutectic point [21,53]. An interesting phenomenon concerning the hydrogen release of Cr coated Zr alloys should be mentioned at this stage: a series of transient test from 1000 °C to 1600 °C were performed in KIT [150,151]. Three sharp increases of hydrogen release were observed during the transient test, as shown in Fig. 26. The first sharp increase at ~1350 °C is owing to the failure of the outer protective Cr_2O_3 scale owing to the Zr-Cr eutectic reaction. The second fast increase at ~1500 °C is due to the transformation of t-ZrO_2 to c-ZrO_2, which leads to the dense columnar grains transfer into bulk equiaxed grains. The third sharp increase at ~1570 is caused by the sudden oxidation of the newly exposed metals by the fracture of the specimens.
Stage 3: During cooldown to room temperature, the Widmanstätten structure is formed by the β-Zr to α-Zr phase transition and residual $ZrCr_2$ intermetallic phase precipitated. As introduced above, the eutectic liquid was absorbed to some active sites in the Zr substrate due to the capillary effect. The volume expansion from liquid phase to solid phase led to the formation of some blisters at the outer surface of the cladding. Fig. 27 shows the macro morphology of Cr coated Zr alloy after the steam oxidation test at 1400 °C for 5 min. It can be seen that some blisters formed on the samples surface. As for the Zr substrate, it has been proved that the structure at the liquid eutectic zone and the Cr-depleted zone is the same: a ZrO_2 layer, an α-Zr(O) layer and a β-Zr layer from outside to inside. The high temperature oxidation mechanism and kinetics is not apparently affected by the formation of the liquid Cr-Zr phase.

The Cr-Zr eutectic reaction makes the Cr coated Zr alloy quite threatened when the accident temperature exceeds 1330 °C. A promising method is to add a barrier between the Cr coating and the Zr substrate, with a eutectic temperature higher than that between chromium and zirconium. Owing to the high melting point of molybdenum (2623 °C), the Cr-Mo and Zr-Mo eutectic temperature is about 1900 °C and 1500 °C, respectively. As already introduced in the Section 2.4, a molybdenum layer has been tried to use by Michau et al. [127] as the interlayer to improve the melting point of Cr coated Zr alloys. Results show that the Cr-Mo coated Zr alloy is still stable after annealing in steam environment at 1400 °C for 300 s. No ZrO_2 layer was found in the Zr substrate after the annealing, indicating that the Cr coating is still protective. As a contrast, a 90 μm ZrO_2 layer formed on the Cr coated Zr alloy specimen after annealing at the same environment for only 100 s. However, the barrier should be chemical stable, with no reaction between Cr or Zr. The applying of Mo as the diffusion barrier seems challenging because of the formation of a thick Zr-Mo interlayer after annealing. Other studies concerning the barrier between the Cr coating and the Zr substrate, such as CrN layer [129], ZrO2 layer [130], does not discuss the coating behavior at the temperature beyond 1400 °C.

6.2. Pre-existing cracks

An ideal coating should be homogeneous, dense and defect-free. Nevertheless, local defects (cracking, checking or tin-holes) can be induced by some external factors such as coating methods, processing parameters and operation environment. Local cracks could be a short path for the diffusion of oxygen, resulting in the accelerated oxidation of the coated cladding. For instance, Fig. 28 shows the cross-section morphology of Cr coated Zr alloy specimens with pre-existence cracks after exposing in steam environment [42,152]. Localized oxidation of both the Cr coating and the Zr substrate was induced by a pre-existing crack within the Cr coating. As a result, a nodular ZrO_2 spot with the thickness of about 10 μm and an α-Zr(O) ring with the thickness of about 20 μm was formed in the Zr substrate. It can be seen that the pre-existing crack was closed by the newly formed chromia, and the residual Cr coating layers were still

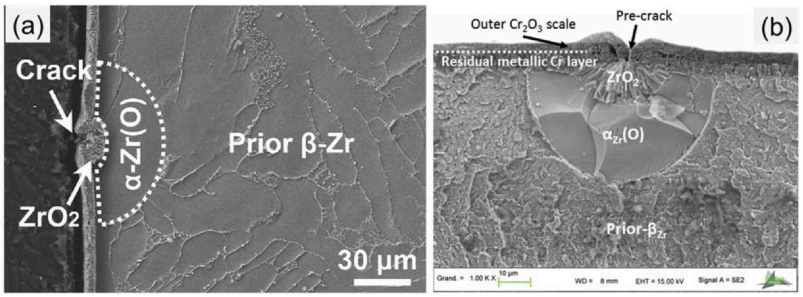

Fig. 28. SEM morphology of Cr-coated Zr alloy specimens with pre-existence cracks after exposure in steam environment for (a) 30 min at 1100 °C and (b) 300 s at 1200 °C .Reproduced with permission from Ref. [152] and Ref. [42].

remarkably fully adherent to the Zr substrate. However, the localized oxidation of the Zr substrate led to the increase of brittleness and the decrease of strength. Due to the temperature increase and core pressure decline in LOCA conditions [140], ballooning and rupture of the cladding tubes may firstly occur at the localized oxidation zone. Xu et al. [153] established a model of coated Zr alloy cladding to study the effect of pre-existing cracks on the mechanical performance of the cladding materials. Results show that the stress field at crack tip in the coating directly lead to the failure of the cladding if the length of the crack reaches a critical value, which is determined by the coating thickness and coating materials.

Cracks may appear in the Cr coating due to its inability to tolerate higher plastic strain in the process of ballooning in LOCA accident. Usually, this type of cracks occurs in the first stage of LOCA, which is ahead of the high temperature steam oxidation process. In order to investigate the effect of the cracks in the coating induced by ballooning, scratches were created by Červenkaa et al. [139] in the coating. Oxidation tests of the scratched Cr coating samples did not show obvious oxidation phenomenon through the coating. But the protecting effect of the coating is also determined by the coating thickness. Similar results were reported by Roache et al. [137]. They even proposed that the pre-existing cracks in the coating may be a useful means to dissipate stress during oxide formation and the ensuing volume expansion, which can further prevent the degradation of the coating. Moreover, the effect of temperature on the self-healing ability of the coating with pre-existence cracks were studied by Ma et al. [152] They found the critical temperature for the large proportion of cracks owing the self-healing ability is 1000 °C.

6.3. Ballooning

Ballooning of the coated cladding tubes in LOCA and beyond LOCA conditions is caused by the inner pressure from the fission gases. The Zr alloy nearly completely loses it strength at temperatures when the α to β phase transformation occurs at about 850 °C. Therefore, the tube is hard to withstand the inner pressure in severe accident conditions, resulting in ballooning or even cladding tubes rapture, which causes a redistribution of fuel to the bottom of the pressure vessel that reduces the cooling ability of the reactor core. The ballooning of the coated cladding tube caused by inner pressure is an issue because of the different extent of deformation of the coating and the substrate. Cracks may form in the coating due to the local stress concentration, and then the accelerated oxidation of the coating occurred due to the fast diffusion of oxygen through the crack. Moreover, the inner surface of the cladding tubes, which is uncoated, will be exposed in high temperature steam environment if burst of the cladding tube occurs, resulting in the oxidation of the inner surface of the cladding tubes and additional hydrogen production. Therefore, it is also important to restrain the fast oxidation and hydrogen release of the inner surface of the cladding tube. DLCVD method has been used by Michau et al. [15,82] to prepare coatings on the inner surface of the cladding tubes.

6.4. Formation of bubbles/blisters/voids

The formation of bubbles/blisters/voids between the Cr coating and the Zr substrate may cause the failure of the coating during high temperature oxidation process, which has been discussed by various researchers. The mismatch of volume expansions of the coating, the substrate and the newly formed oxide layer is the main reason for the formation of bubbles.

Firstly, some blisters are found between the coating and the Cr_2O_3 layer, of which the diameters are relatively smaller. A typical blister morphology is shown in Fig. 29(a). Considering the fact that the Pilling-Bedworth ratio of Cr_2O_3 is 2.07 [154], the strong volume expansion during oxidation causes the increasing of compressive stress of the coating during high temperature exposure process. Then, the large difference in the thermal expansion coefficients for Cr_2O_3 (9.6×10^{-6}/K), Cr (6.5×10^{-6}/K) and Zr ($5.77–7.62 \times 10^{-6}$/K) during cool-down process results in the formation of the bubbles/blisters/voids. Such phenomenon has been reported by many researches [25,42,51,68,79].

Another type of bubbles is observed at the interface between the Cr-Zr interlayer and the Zr substrate [25,74]. Fig. 29(b) shows the cross-section morphology of a Cr coated Zr alloy sample after annealing in air environment at 1200 °C for 3 h, which was reported by Wei et al. [25]. The size of this type of bubbles is obviously larger than that of the first one, and the location of the bubbles is different. The explanation by the authors is based on the volume expansion of the Zr substrate due to the phase transformation of Zr, namely the

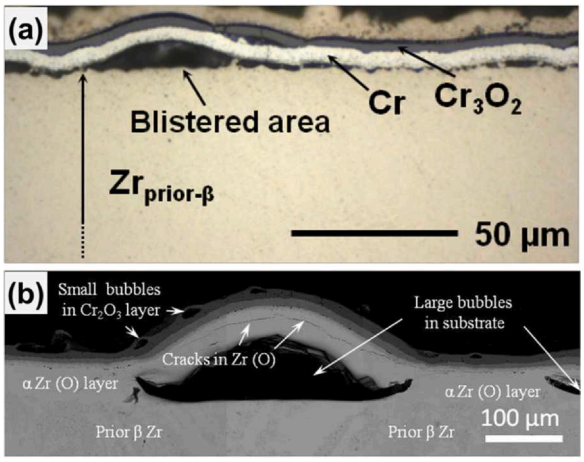

Fig. 29. Surface and the cross-section morphology of a Cr coated Zr alloy sample after annealing at 1200 °C for 3 h. Bubbles were observed on the Cr coating surface after oxidation tests. Reproduced with permission from Ref. [42] and Ref. [25].

formation of α-Zr(O) layer with a relatively higher volume. It is widely accepted that the structure of bare Zr alloys after exposure in LOCA conditions includes an α-Zr(O) layer, a ZrO_2 layer and a prior β-Zr layer [43]. As for the Cr coated Zr alloys, although the existence of the Cr coating hindered the diffusing of oxygen from the atmosphere to the Zr substrate, an α-Zr(O) layer was still observed beneath the Cr-Zr interlayer after exposing in steam environment [155,156] or even after annealing in inert gas environment [104] at 1200 °C. The volume expansion due to the phase transformation from β-Zr to α-Zr (O) was restrained by the Cr coating, and the differences of mechanical properties (hardness and ductility) between the β-Zr and the α-Zr(O) make the phase interface the weak site. As a result, micro cracks formed at the interface between the β-Zr and the α-Zr(O). And bubbles formed when the micro cracks gathered together. In the end, the broken of the bubbles caused the failure of the Cr coating. It should be emphasized that the works by Wei et al. [25] and Hu et al. [79] were done in air condition. Seldom researches in steam environment show similar bubble phenomenon, which could be due to the existence of nitrogen gas. The nitrogen gas in air can apparently affect the oxidation process of Cr coatings because the nitrogen affinity of Zr and Cr is both very high [157].

Moreover, according to the EDS mapping results of the cross section of Cr coated Zr alloy sample after annealing [79], the Sn/Cr segregation was found on both the first and the second type of the voids, indicating that the formation of the voids is caused by Elemental segregation and separation.

6.5. Local oxidation of welding zone

A nuclear fuel rod consists two end plugs, which are joined with cladding tubes by welding. The end plugs should also be deposited to form a protective coating. The special geometry of the connecting part between the cladding tube and the end plug makes it hard to get a uniform coating on it, making it the weak point of the whole fuel rod in accident conditions. An air oxidation experiment on fully Cr-coated Zr alloy cladding tubes was conducted by Sidelev et al. [158] to evaluate the effect of resistance upset welding. Partially oxidation enhancement is found at the weld burr region: the Cr coating at the weld burr region totally disappears, oxygen and nitrogen have diffused into the Zr substrate, forming solutions of α-Zr (O) and α-Zr(N). The weak part could result in failure of the whole cladding tube. Additional treatment method such as mechanical processing should be used to get a relatively smooth surface of the nuclear fuel rod after welding.

7. Outlook

With the increased number of researches on Cr coated Zr alloys ATF cladding materials, the understanding of oxidation, diffusion and mechanical behavior of the coated cladding in LOCA and beyond LOCA conditions becomes deeper and deeper. Unfortunately, there are still some questions to be figured out before the commercial use of the Cr coating. Until extensive long-time and comprehensive studies have not been done, a too optimistic attitude rather hinders the commercial use of Cr coated Zr alloys ATF cladding materials inside reactor core. Some critical questions are listed:

(1). How to estimate the "survival time" of the coated cladding in DBA or BDBA conditions?

The aim of depositing a protective coating on the Zr alloy surface is to increase the coping time for accident management measures, so the duration that the coating remain its protective is an important parameter to evaluate the coating quality. However, it is hard to accurately estimate the "survival time" of the coated cladding in LOCA or beyond LOCA conditions. Up to now, the common method for the coating survival time estimation is to obtain the oxidation kinetics of the Cr coating, and then calculate the time that the Cr coating is totally oxidized Cr_2O_3. Moreover, a considerable part of the coating is consumed by diffusing and dissolving in the Zr substrate in high temperature environment, and a universal consumption kinetics of the coating including the oxidation part and the diffusion part was used for the coating survival time estimation [42,68,104]. The accelerated oxidation of the coated cladding may occur although the residual coating remained (e.g., the formation of cracks or the formation of intergranular ZrO_2), making it hard to estimate the survival time of the coating in LOCA conditions. In short, no convincible model can be used for now to estimate the survival time of the Cr coating in LOCA or beyond LOCA conditions. A model that can precisely evaluate the survival time of the coating based on the exposure temperature, coating thickness and alloying elements should be given in the future.

(2). What is the coupling effect of stress generation and oxidation reaction on the failure of the coating in LOCA environment?

As introduced in the Section 3.1, the cladding tube is under tensile stress when a loss of coolant accident occurs. Indeed, the diffusion rate, diffusion path of oxidizing species in the coating may be affected by the stress state of the materials [159,160]. Moreover, the formation mechanism of cracks in the coating is significantly affected by the stress state of the coating. However, most of the oxidation tests done in the past have been performed with coupon samples and thus do not take into account of the effect of stress conditions, which is due to the difficulty of the stress loading in extreme high temperature environment. Indeed, the stress condition should be considered when evaluating the quality of a Cr coating in the future. The coupling effect of tensile stress and oxidation reaction on the crack evolution in the coating should be clarified.

(3). Which material can be used as a diffusion barrier between the Cr coating and the Zr substrate?

As introduced in Section 2.2, a considerable part of the Cr coating is consumed by diffusing and dissolving in the Zr substrate in high temperature environment. In addition, the Cr-Zr eutectic reaction at 1332 °C can lead to the fast failure of the coating in BDBA environment. In order to avoid this destruction of Cr coating by the direct contact of the Cr coating and the Zr substrate, a diffusion barrier is favored between the Cr coating and the Zr substrate. The solubility of the element as the diffusion barrier in the zirconium substrate should be lower than that of chromium, and the eutectic temperature between the new element and zirconium should be as high as possible. Further studies should be done to find out what materials can be used as the diffusion barrier.

(4). Is the adhesion property of the Cr coating affected by the Kirkendall type cavities between the Cr-Zr interlayer and the Zr substrate?

After exposing in high temperature steam environment for a while, some cavities formed between the Cr-Zr interlayer and the Zr substrate in the Cr coated Zr alloys. The formation mechanism of the cavities is based on a Kirkendall-type mechanism, which refers to the movement of diffusion interface due to the difference on relative diffusion velocity of the atoms. Although most of the researches show that no spallation phenomenon of the Cr coating was found after oxidation tests of the coated alloys, however, most of the studies were done in stress-free condition. Whether the cavities can affect adhesion property of the Cr coating in real LOCA conditions (high temperature steam, tensile stress, irradiation) is still unknown.

(5). A standard test method for the oxidation behavior in LOCA conditions is needed.

Although tremendous amounts of oxidation tests have been done to evaluate the oxidation resistance of the Cr coating Zr alloy

cladding materials, the test methods and test conditions are different. The typical test facilities are thermogravimetries and tube furnaces, which own different heating up time. The Typical test environment is steam environment, but the H_2O percentage and the steam flux of the tests by different studies are different. Moreover, the adherent properties of tube samples and cubic samples are different, which may also affect the oxidation behavior of the coating. In a word, a standard test method for the oxidation behavior in LOCA conditions is needed, which means the annealing temperature, duration, steam flux, test facility, heating up time, shape of the specimen for the coating evaluation test should be unified. Only in this way, the quality of the coating prepared by different research group around the world can be distinctively compared.

Recently, the OECD-NEA Joint Undertaking project "QUENCH-ATF" was started in KIT, which is aimed to investigate the chemical, mechanical and thermal-hydraulics behavior of ATF claddings in DBA and BDBA scenarios. This will be achieved through a series of three bundle tests at the QUENCH facility at KIT. The QUENCH facility is dedicated to DBA-LOCA experiments with pressurized fuel rod simulators and early in-vessel severe accident scenarios with reflood occurring from high temperatures. Within the framework of this project, two or three large-scale bundle tests with Cr coated cladding tubes will be conducted. Behaviors of the Cr coating Zr alloy cladding tubes in realistic thermal-hydraulic boundary conditions, which considering the feedback of chemical heat release on temperature progression, the heat transfer and interactions between rods, the influence of grid spacers, and the real 2-phase flow cooling water, will be investigated and discussed.

Declaration of Competing Interest

The authors declare that they have no known competing financial interests or personal relationships that could have appeared to influence the work reported in this paper.

Acknowledgements

Funding: This work was supported by the Projects from the National Natural Science Foundation of China [52101096].

References

[1] S.J. Zinkle, G. Was, Materials challenges in nuclear energy, Acta Mater. 61 (2013) 735–758.
[2] K.A. Terrani, S.J. Zinkle, L.L. Snead, Advanced oxidation-resistant iron-based alloys for LWR fuel cladding, J. Nucl. Mater. 448 (2014) 420–435.
[3] K.A. Terrani, Accident tolerant fuel cladding development: Promise, status, and challenges, J. Nucl. Mater. 501 (2018) 13–30.
[4] L.J. Ott, K.R. Robb, D. Wang, Preliminary assessment of accident-tolerant fuels on LWR performance during normal operation and under DB and BDB accident conditions, J. Nucl. Mater. 448 (2014) 520–533.
[5] K.R. Robb, Analysis of the FeCrAl accident tolerant fuel concept benefits during BWRstation blackout accidents, in, Oak Ridge National Lab.(ORNL), Oak Ridge, TN(United States), 2015.
[6] M.T. Farmer, L. Leibowitz, K.A. Terrani, K.R. Robb, Scoping assessments of ATF impact on late-stage accident progression including molten core–concrete interaction, J. Nucl. Mater. 448 (2014) 534–540.
[7] B.J. Merrill, S.M. Bragg-Sitton, P.W. Humrickhouse, Modification of MELCOR for severe accident analysis of candidate accident tolerant cladding materials, Nucl. Eng. Des. 315 (2017) 170–178.
[8] E. Kashkarov, B. Afornu, D. Sidelev, M. Krinitcyn, V. Gouws, A. Lider, Recent advances in protective coatings for accident tolerant Zr-based fuel claddings, Coatings 11 (2021) 557.
[9] C. Tang, M. Stueber, H.J. Seifert, M. Steinbrueck, Protective coatings on zirconium-based alloys as accident-tolerant fuel (ATF) claddings, Corros. Rev. 35 (2017) 141–165.
[10] C. Tang, M. Klimenkov, U. Jaentsch, H. Leiste, M. Rinke, S. Ulrich, M. Steinbrück, H.J. Seifert, M. Stueber, Synthesis and characterization of Ti2AlC coatings by magnetron sputtering from three elemental targets and ex-situ annealing, Surf. Coat. Technol. 309 (2017) 445–455.
[11] C. Tang, M. Steinbrück, M. Große, T. Bergfeldt, H.J. Seifert, Oxidation behavior of Ti2AlC in the temperature range of 1400 °C–1600 °C in steam, J. Nucl. Mater. 490 (2017) 130–142.
[12] C. Tang, M. Steinbrueck, M. Stueber, M. Grosse, X. Yu, S. Ulrich, H.J. Seifert, Deposition, characterization and high-temperature steam oxidation behavior of single-phase Ti2AlC-coated Zircaloy-4, Corros. Sci. 135 (2018) 87–98.
[13] M.A. Tunes, R.W. Harrison, S.E. Donnelly, P.D. Edmondson, A. Transmission, Electron microscopy study of the neutron-irradiation response of Ti-based MAX phases at high temperatures, Acta Mater. 169 (2019) 237–247.
[14] C. Tang, M. Große, S. Ulrich, M. Klimenkov, U. Jäntsch, H.J. Seifert, M. Stüber, M. Steinbrück, High-temperature oxidation and hydrothermal corrosion of textured Cr2AlC-based coatings on zirconium alloy fuel cladding, Surf. Coat. Technol. 419 (2021) 127263.
[15] A. Michau, F. Maury, F. Schuster, I. Nuta, Y. Gazal, R. Boichot, M. Pons, Chromium carbide growth by direct liquid injection chemical vapor deposition in long and narrow tubes, experiments, modeling and simulation, Coatings 8 (2018) 220.
[16] J.G. Gigax, M. Kennas, H. Kim, T. Wang, B.R. Maier, H. Yeom, G.O. Johnson, K. Sridharan, L. Shao, Radiation response of Ti2AlC MAX phase coated Zircaloy-4 for accident tolerant fuel cladding, J. Nucl. Mater. 523 (2019) 26–32.
[17] W. Xiao, H. Deng, S. Zou, Y. Ren, D. Tang, M. Lei, C. Xiao, X. Zhou, Y. Chen, Effect of roughness of substrate and sputtering power on the properties of TiN coatings deposited by magnetron sputtering for ATF, J. Nucl. Mater. 509 (2018) 542–549.
[18] M.A. Tunes, F.C. da Silva, O. Camara, C.G. Schön, J.C. Sagás, L.C. Fontana, S.E. Donnelly, G. Greaves, P.D. Edmondson, Energetic particle irradiation study of TiN coatings: are these films appropriate for accident tolerant fuels? J. Nucl. Mater. 512 (2018) 239–245.
[19] E. Alat, A.T. Motta, R.J. Comstock, J.M. Partezana, D.E. Wolfe, Multilayer (TiN, TiAlN) ceramic coatings for nuclear fuel cladding, J. Nucl. Mater. 478 (2016) 236–244.
[20] O.V. Maksakova, R.F. Webster, R.D. Tilley, V.I. Ivashchenko, B.O. Postolnyi, O.V. Bondar, Y. Takeda, V.M. Rogoz, R.E. Sakenova, P.V. Zukowski, M. Opielak, V.M. Beresnev, A.D. Pogrebnjak, Nanoscale architecture of (CrN/ZrN)/(Cr/Zr) nanocomposite coatings: Microstructure, composition, mechanical properties and first-principles calculations, J. Alloy. Compd. 831 (2020) 154808.
[21] J. Brachet, T. Guilbert, M. Le Saux, J. Rousselot, G. Nony, C. Toffolon-Masclet, A. Michau, F. Schuster, H. Palancher, J. Bischoff, Behavior of Cr-coated M5 claddings during and after high temperature steam oxidation from 800 C up to 1500 C (Loss-of-Coolant Accident & Design Extension Conditions), in: Proceedings of the Topfuel 2018, Prague, Czech Republic, 2018.
[22] X. Han, J. Xue, S. Peng, H. Zhang, An interesting oxidation phenomenon of Cr coatings on Zry-4 substrates in high temperature steam environment, Corros. Sci. 156 (2019) 117–124.
[23] H.-G. Kim, I.-H. Kim, Y.-I. Jung, D.-J. Park, J.-Y. Park, Y.-H. Koo, High-temperature oxidation behavior of Cr-coated zirconium alloy, in: Proceedings of the LWR Fuel Performance Meeting/TopFuel, Charlotte, USA, 2013, 842–846.
[24] Y. Wang, W. Zhou, Q. Wen, X. Ruan, F. Luo, G. Bai, Y. Qing, D. Zhu, Z. Huang, Y. Zhang, T. Liu, R. Li, Behavior of plasma sprayed Cr coatings and FeCrAl coatings on Zr fuel cladding under loss-of-coolant accident conditions, Surf. Coat. Technol. 344 (2018) 141–148.
[25] T. Wei, R. Zhang, H. Yang, H. Liu, S. Qiu, Y. Wang, P. Du, K. He, X. Hu, C. Dong, Microstructure, corrosion resistance and oxidation behavior of Cr-coatings on Zircaloy-4 prepared by vacuum arc plasma deposition, Corros. Sci. 158 (2019) 108077.
[26] Z. Yang, Y. Niu, J. Xue, T. Liu, C. Chang, X. Zheng, Steam oxidation resistance of plasma sprayed chromium-containing coatings at 1200°C, Mater. Corros. 70 (2019) 37–47.
[27] M. Lenling, H. Yeom, B. Maier, G. Johnson, T. Dabney, J. Graham, P. Hosemann, D. Hoelzer, S. Maloy, K. Sridharan, Manufacturing oxide dispersion-strengthened (ODS) steel fuel cladding tubes using the cold spray process, JOM 71 (2019) 2868–2873.
[28] J.-M. Kim, T.-H. Ha, I.-H. Kim, H.-G. Kim, Microstructure and oxidation behavior of CrAl laser-coated Zircaloy-4 alloy, Metals 7 (2017) 59.
[29] J.-M. Kim, T.-H. Ha, J.-S. Park, H.-G. Kim, Effect of laser surface treatment on the corrosion behavior of FeCrAl-coated TZM alloy, Metals 6 (2016) 29.
[30] C.P. Massey, K.A. Terrani, S.N. Dryepondt, B.A. Pint, Cladding burst behavior of Fe-based alloys under LOCA, J. Nucl. Mater. 470 (2016) 128–138.
[31] X. Li, C. Meng, X. Xu, X. He, C. Wang, Effect of Al content on high-temperature oxidation behavior and failure mechanism of CrAl-coated Zircaloy, Corros. Sci. 192 (2021) 109856.
[32] N. Sekido, K. Soeta, K. Yoshimi, Liquidus projection and solidification paths in the Zr-Si-Al ternary system, J. Alloy. Compd. 885 (2021) 160911.
[33] P. Richardson, D. Cuskelly, M. Brandt, E. Kisi, Microstructural analysis of in-situ reacted Ti2AlC MAX phase composite coating by laser cladding, Surf. Coat. Technol. 385 (2020) 125360.
[34] Y. Lei, L. Chen, J. Zhang, F. Xue, G. Bai, Y. Zhang, T. Liu, R. Li, S. Li, J. Wang, Influence of Al concentration on mechanical property and oxidation behavior of Zr-Al-C coatings, Surf. Coat. Technol. 372 (2019) 65–71.
[35] Y. Al-Olayyan, G.E. Fuchs, R. Baney, J. Tulenko, The effect of Zircaloy-4 substrate surface condition on the adhesion strength and corrosion of SiC coatings, J. Nucl. Mater. 346 (2005) 109–119.
[36] C. Meng, L. Yang, Y. Wu, J. Tan, W. Dang, X. He, X. Ma, Study of the oxidation behavior of CrN coating on Zr alloy in air, J. Nucl. Mater. 515 (2019) 354–369.
[37] J. Krejčí, J. Kabátová, F. Manoch, J. Kočí, L. Cvrček, J. Málek, S. Krum, P. Šutta, P. Bublíková, P. Halodová, H.K. Namburi, M. Ševeček, Development and testing of multicomponent fuel cladding with enhanced accidental performance, Nucl. Eng. Technol. 52 (2020) 597–609.
[38] X. Han, Y. Wang, S. Peng, H. Zhang, Oxidation behavior of FeCrAl coated Zry-4 under high temperature steam environment, Corros. Sci. 149 (2019) 45–53.

[39] W. Zhong, P.A. Mouche, X. Han, B.J. Heuser, K.K. Mandapaka, G.S. Was, Performance of iron–chromium–aluminum alloy surface coatings on Zircaloy 2 under high-temperature steam and normal BWR operating conditions, J. Nucl. Mater. 470 (2016) 327–338.

[40] B.A. Pint, K.A. Terrani, M.P. Brady, T. Cheng, J.R. Keiser, High temperature oxidation of fuel cladding candidate materials in steam–hydrogen environments, J. Nucl. Mater. 440 (2013) 420–427.

[41] G. Jiang, D. Xu, P. Feng, S. Guo, J. Yang, Y. Li, Corrosion of FeCrAl alloys used as fuel cladding in nuclear reactors, J. Alloy. Compd. 869 (2021) 159235.

[42] J.-C. Brachet, I. Idarraga-Trujillo, M. Le Flem, M. Le Saux, V. Vandenberghe, S. Urvoy, E. Rouesne, T. Guilbert, C. Toffolon-Masclet, M. Tupin, C. Phalippou, F. Lomello, F. Schuster, A. Billard, G. Velisa, C. Ducros, F. Sanchette, Early studies on Cr-Coated Zircaloy-4 as enhanced accident tolerant nuclear fuel claddings for light water reactors, J. Nucl. Mater. 517 (2019) 268–285.

[43] M. Steinbrück, N. Vér, M. Große, Oxidation of advanced zirconium cladding alloys in steam at temperatures in the range of 600–1200 °C, Oxid. Met. 76 (2011) 215–232.

[44] H.-G. Kim, I.-H. Kim, Y.-I. Jung, D.-J. Park, J.-Y. Park, Y.-H. Koo, Adhesion property and high-temperature oxidation behavior of Cr-coated Zircaloy-4 cladding tube prepared by 3D laser coating, J. Nucl. Mater. 465 (2015) 531–539.

[45] F. Qi, Z. Liu, Q. Li, H. Yu, P. Chen, Y. Li, Y. Zhou, C. Ma, C. Tang, Y. Huang, B. Zhao, H. Lu, Pellet-cladding mechanical interaction analysis of Cr-coated Zircaloy cladding, Nucl. Eng. Des. 367 (2020) 110792.

[46] D. Arias, J.J.Bo.A.P.D. Abriata, TheCr– Zr (Chromium-Zirconium) system, Bull. Alloy Phase Diagr. 7 (1986) 237–244.

[47] R.V. Umretiya, B. Elward, D. Lee, M. Anderson, R.B. Rebak, J.V. Rojas, Mechanical and chemical properties of PVD and cold spray Cr-coatings on Zircaloy-4, J. Nucl. Mater. 541 (2020) 152420.

[48] J. Bischoff, C. Vauglin, C. Delafoy, P. Barberis, D. Perche, B. Guerin, J. Vassault, J.J. P.T.F. Brachet, Development of Cr-coated Zirconium Alloy Cladding for Enhanced Accident Tolerance, (2016)1165–1171.

[49] R. Oelrich, S. Ray, Z. Karoutas, P. Xu, J. Romero, H. Shah, E. Lahoda, F. Boylan, Overview of westinghouse lead accident tolerant fuel program, in: Proceedings of the TOP FUEL 2018 Conference, Prague, Czech Republic, 30 September–4 October, 2018, A0036.

[50] I. Idarraga-Trujillo, M. Le Flem, J.-C. Brachet, M. Le Saux, D. Hamon, S. Muller,V. Vandenberghe, M. Tupin, E. Papin, E.J.T.F. Monsifrot, Assessment at CEA of coated nuclear fuel cladding for LWRs with increased margins in LOCA and beyond LOCA conditions, 2 (2013) 15–19.

[51] H. Liu, Y. Feng, Y. Yao, B. Li, R. Wang, X. Shi, P. Li, J. Shu, F. Huang, Q. Huang, F. Ge, Effect of the 345 °C and 16.5 MPa autoclave corrosion on the oxidation behavior of Cr-coated zirconium claddings in the high-temperature steam, Corros. Sci. 189 (2021) 109608.

[52] J. Brachet, M. Le Saux, M. Le Flem, S. Urvoy, E. Rouesne, T. Guilbert, C. Cobac, F. Lahogue, J. Rousselot, M. Tupin, On-going studies at CEA on chromium coated zirconium based nuclear fuel claddings for enhanced accident tolerant LWRs fuel, in: Proceedings of, 2015, 13–19.

[53] M. Ševeček, A. Gurgen, A. Seshadri, Y. Che, M. Wagih, B. Phillips, V. Champagne, K. Shirvan, Development of Cr cold spray–coated fuel cladding with enhanced accident tolerance, Nucl. Eng. Technol. 50 (2018) 229–236.

[54] M. Yao, X. Zhang, K. Hou, J. Zhang, P. Hu, J. Peng, B. Zhou, The initial corrosion behavior of Zr-0.75Sn-0.35Fe-0.15Cr alloy in deionized water at 250 ℃, Acta Metall. Sin. 56 (2020) 221–230.

[55] W.G. Cook, R.P. Olive, Pourbaix diagrams for chromium, aluminum and titanium extended to high-subcritical and low-supercritical conditions, Corros. Sci. 58 (2012) 291–298.

[56] V. Kolarik, M. Wagner, B. Michelfelder, Corrosion of Alloys 625 and pure chromium in Cl-containing fluids during supercritical water oxidation (SCWO), in: Proceedings of the Corrosion 99, 1999.

[57] J.Q. Yang, S.Z. Wang, X.Y. Tang, Y.Z. Wang, Y.H. Li, Effect of low oxygen concentration on the oxidation behavior of Ni-based alloys 625 and 825 in supercritical water, J. Supercrit. Fluids 131 (2018) 1–10.

[58] J.Q. Yang, S.Z. Wang, D.H. Xu, High temperature oxidation of alloy 617, 740, HR6W and Sanicro 25 in supercritical water at 650 °C, Corros. Eng. Sci. Technol. 55 (2020) 196–204.

[59] P. Kritzer, N. Boukis, E. Dinjus, Review of the corrosion of nickel-based alloys and stainless steels in strongly oxidizing pressurized high-temperature solutions at subcritical and supercritical temperatures, Corrosion 56 (2000) 1093–1104.

[60] M.C. Sun, X.Q. Wu, Z.E. Zhang, E.H. Han, Analyses of oxide films grown on Alloy 625 in oxidizing supercritical water, J. Supercrit. Fluids 47 (2008) 309–317.

[61] G. Girardin, R. Meier, F. Jatuff, J. Bischoff, C. Delafoy, E.J.P.o.T. Schweitzer, Inspection Capabilities and In-pile Experience with Innovative and EnhancedAccident Tolerant Fuel Materials at KKG, (2018).

[62] L. Royer, X. Ledoux, S. Mathieu, P. Steinmetz, On the oxidation and nitridation of chromium at 1300C, Oxid. Met. 74 (2010) 79–92.

[63] M. Michalik, M. Hänsel, J. Zurek, L. Singheiser, W. Quadakkers, Effect of water vapour on growth and adherence of chromia scales formed on Cr in high and low pO2-environments at 1000 and 1050 C, Mater. High Temp. 22 (2005) 213–221.

[64] E.J. Opila, N.S. Jacobson, D.L. Myers, E.H. Copland, Predicting oxide stability in high-temperature water vapor, JOM 58 (2006) 22–28.

[65] S.K. Arifin, M. Hamid, A.N. Berahim, M.H. Ani, Effects of water vapor on protectiveness of Cr_2O_3 scale at 1073 K, in: Proceedings of the IOP Conference Series: Materials Science and Engineering, 290 (2018) 012085.

[66] Q. Chen, Y. Xiang, Z. Li, H. He, Y. Zhong, C. Zhu, N. Liu, Y. Yang, J. Liao, H. Chang, C. Liu, J. Yang, Microstructure evolution and adhesion properties of thick Cr coatings under different thermal shock temperatures, Surf. Coat. Technol. 417 (2021) 127224.

[67] J.-C. Brachet, E. Rouesne, J. Ribis, T. Guilbert, S. Urvoy, G. Nony, C. Toffolon-Masclet, M. Le Saux, N. Chaabane, H. Palancher, A. David, J. Bischoff, J. Augereau, E. Pouillier, High temperature steam oxidation of chromium-coated zirconium-based alloys: Kinetics and process, Corros. Sci. 167 (2020) 108537.

[68] H. Yeom, B. Maier, G. Johnson, T. Dabney, M. Lenling, K. Sridharan, High temperature oxidation and microstructural evolution of cold spray chromium coatings on Zircaloy-4 in steam environments, J. Nucl. Mater. 526 (2019) 151737.

[69] M.M. Groβe, K. Van Loo, E.L. Frankberg, C. Tang, K. Lambrinou, F. Di Fonzo, M. Steinbrück, Investigation of corrosion and high temperature oxidation of promising ATF cladding materials in the framework of the Il trovatore project, in: Proceedings of the Global/Top Fuel 2019: Light Water Reactor Fuel Performance Conference, American Nuclear Society, 2019, 274–279.

[70] M. Hänsel, W.J. Quadakkers, D.J. Young, Role of water vapor in chromia-scale growth at low oxygen partial pressure, Oxid. Met. 59 (2003) 285–301.

[71] E.B. Kashkarov, D.V. Sidelev, M.S. Syrtanov, C. Tang, M. Steinbrück, Oxidation kinetics of Cr-coated zirconium alloy: effect of coating thickness and microstructure, Corros. Sci. 175 (2020) 108883.

[72] J. Krejčí , M. Ševeček , L. Cvrcek , J. Kabátová , F. Manoch , Chromium and chromium nitride coated cladding for nuclear reactor fuel, in: Proceedings of the Twentieth International Corrosion Congress, EUROCORR, 2017.

[73] J.-H. Park, H.-G. Kim, J.-y Park, Y.-I. Jung, D.-J. Park, Y.-H. Koo, , High temperature steam-oxidation behavior of arc ion plated Cr coatings for accident tolerant fuel claddings, Surf. Coat. Technol. 280 (2015) 256–259.

[74] X. He, Z. Tian, B. Shi, X. Xu, C. Meng, W. Dang, J. Tan, X. Ma, Effect of gas pressure and bias potential on oxidation resistance of Cr coatings, Ann. Nucl. Energy 132 (2019) 243–248.

[75] H.-B. Ma, J. Yan, Y.-H. Zhao, T. Liu, Q.-S. Ren, Y.-H. Liao, J.-D. Zuo, G. Liu, M.-Y. Yao, Oxidation behavior of Cr-coated zirconium alloy cladding in high-temperature steam above 1200 °C, npj Mater. Degrad. 5 (2021) 7.

[76] X. Han, C. Chen, Y. Tan, W. Feng, S. Peng, H. Zhang, A systematic study of the oxidation behavior of Cr coatings on Zry4 substrates in high temperature steam environment, Corros. Sci. 174 (2020) 108826.

[77] V.A. Grudinin, G.A. Bleykher, D.V. Sidelev, V.P. Krivobokov, M. Bestetti, A. Vicenzo, S. Franz, Chromium films deposition by hot target high power pulsed magnetron sputtering: Deposition conditions and film properties, Surf. Coat. Technol. 375 (2019) 352–362.

[78] D.V. Sidelev, G.A. Bleykher, M. Bestetti, V.P. Krivobokov, A. Vicenzo, S. Franz, M.F. Brunella, A comparative study on the properties of chromium coatings deposited by magnetron sputtering with hot and cooled target, Vacuum 143 (2017) 479–485.

[79] X. Hu, C. Dong, Q. Wang, B. Chen, H. Yang, T. Wei, R. Zhang, W. Gu, D. Chen, High-temperature oxidation of thick Cr coating prepared by arc deposition for accident tolerant fuel claddings, J. Nucl. Mater. 519 (2019) 145–156.

[80] B.R. Maier, H. Yeom, G. Johnson, T. Dabney, J. Hu, P. Baldo, M. Li, K. Sridharan, In situ TEM investigation of irradiation-induced defect formation in cold spray Cr coatings for accident tolerant fuel applications, J. Nucl. Mater. 512 (2018) 320–323.

[81] H. Yeom, T. Dabney, G. Johnson, B. Maier, M. Lenling, K. Sridharan, Improving deposition efficiency in cold spraying chromium coatings by powder annealing, Int. J. Adv. Manuf. Technol. 100 (2019) 1373–1382.

[82] A. Michau, Y. Gazal, F. Addou, F. Maury, T. Duguet, R. Boichot, M. Pons, E. Monsifrot, H. Maskrot, F. Schuster, Scale up of a DLI-MOCVD process for the internal treatment of a batch of 16 nuclear fuel cladding segments with a CrCx protective coating, Surf. Coat. Technol. 375 (2019) 894–902.

[83] J.C. Brachet, S. Urvoy, E. Rouesne, G. Nony, M. Dumerval, M.L. Saux, F. Ott, A. Michau, F. Schuster, F. Maury, DLI-MOCVD CrxCy coating to prevent Zr-based cladding from inner oxidation and secondary hydriding upon LOCA conditions, J. Nucl. Mater. 550 (2021) 152953.

[84] D.V. Nguyen, M. Le Saux, L. Gélébart, J.-C. Brachet, J.-P. Bonthonneau, A. Courcelle, R. Guillou, E. Rouesne, S. Urvoy, Mechanical behavior of a chromium coating on a zirconium alloy substrate at room temperature, J. Nucl. Mater. (2021) 153332.

[85] A. Fazi, H. Aboulfadl, A.H.S. Iyer, M. Sattari, K.M. Stiller, P. Lokhande, M. Thuvander, H.-O. Andren, Characterization of as-deposited cold sprayed Cr-coating on optimized ZIRLOTM claddings, J. Nucl. Mater. 549 (2021) 152892.

[86] J. Jiang, X. Ma, B. Wang, Positive or negative role of preoxidation in the crack arresting of Cr coating for accident tolerant fuel cladding, Corros. Sci. 193 (2021) 109870.

[87] J. Bischoff, C. Delafoy, N. Chaari, C. Vauglin, K. Buchanan, P. Barberis, E. Monsifrot, F. Schuster, J. Brachet, K. Nimishakavi, Cr-coated cladding development at framatome, Top Fuel 2018 (2018) A0152.

[88] H. Li, B. Jiang, B. Yang, Study on crystalline to amorphous structure transition of Cr coatings by magnetron sputtering, Appl. Surf. Sci. 258 (2011) 935–939.

[89] I. Efeoglu, R.D. Arnell, S.F. Tinston, D.G. Teer, The mechanical and tribological properties of titanium aluminium nitride coatings formed in a four magnetron closed-field sputtering system, Surf. Coat. Technol. 57 (1993) 117–121.

[90] S. Yang, E. Wiemann, D.G. Teer, The properties and performance of Cr-based multilayer nitride hard coatings using unbalanced magnetron sputtering and elemental metal targets, Surf. Coat. Technol. 188–189 (2004) 662–668.

[91] G.A. Bleykher, V.P. Krivobokov, A.V. Yurjeva, I. Sadykova, Energy and substance transfer in magnetron sputtering systems with liquid-phase target, Vacuum 124 (2016) 11–17.

[92] G.A. Bleykher, V.P. Krivobokov, A.V. Yuryeva, Magnetron deposition of coatings with evaporation of the target, Tech. Phys. 60 (2015) 1790–1795.

[93] D.V. Sidelev, E.B. Kashkarov, M.S. Syrtanov, V.P. Krivobokov, Nickel-chromium (Ni–Cr) coatings deposited by magnetron sputtering for accident tolerant nuclear fuel claddings, Surf. Coat. Technol. 369 (2019) 69–78.

[94] Q.S. Chen, C.H. Liu, R.Q. Zhang, H.Y. Yang, T.G. Wei, Y. Wang, Z. Li, L.X. He, J. Wang, L. Wang, J.P. Long, H. Chang, Microstructure and high-temperature steam oxidation properties of thick Cr coatings prepared by magnetron sputtering for accident tolerant fuel claddings: the role of bias in the deposition process, Corros. Sci. 165 (2020) 108378.

[95] Y. Meng, S. Zeng, Z. Teng, X. Han, H. Zhang, Control of the preferential orientation Cr coatings deposited on zircaloy substrates and study of their oxidation behavior, Thin Solid Films 730 (2021) 138699.

[96] B. Maier, H. Yeom, G. Johnson, T. Dabney, J. Walters, J. Romero, H. Shah, P. Xu, K. Sridharan, Development of cold spray coatings for accident-tolerant fuel cladding in light water reactors, JOM 70 (2018) 198–202.

[97] B. Maier, H. Yeom, G. Johnson, T. Dabney, J. Walters, P. Xu, J. Romero, H. Shah, K. Sridharan, Development of cold spray chromium coatings for improved accident tolerant zirconium-alloy cladding, J. Nucl. Mater. 519 (2019) 247–254.

[98] X.-T. Luo, C.-X. Li, F.-L. Shang, G.-J. Yang, Y.-Y. Wang, C.-J. Li, High velocity impact induced microstructure evolution during deposition of cold spray coatings: a review, Surf. Coat. Technol. 254 (2014) 11–20.

[99] P.C. King, S.H. Zahiri, M. Jahedi, Microstructural refinement within a cold-sprayed copper particle, Metall. Mater. Trans. A 40 (2009) 2115–2123.

[100] C. Gautier, J. Machet, Effects of deposition parameters on the texture of chromium films deposited by vacuum arc evaporation, Thin Solid Films 289 (1996) 34–38.

[101] J. Huang, S. Zou, W. Xiao, C. Yang, D. Tang, H. Yu, L. Zhang, K. Zhang, Influences of arc current on microstructure of Cr coating for Zr-4 alloy prepared by multi-arc ion plating via EBSD, Mater. Charact. 178 (2021) 111211.

[102] Z. Duan, H. Yang, Y. Satoh, K. Murakami, S. Kano, Z. Zhao, J. Shen, H. Abe, Current status of materials development of nuclear fuel cladding tubes for light water reactors, Nucl. Eng. Des. 316 (2017) 131–150.

[103] Z.B. Yang, J.J. Liao, S.Y. Qiu, Z.Q. Cheng, H. Liu, Z.P. Wu, J. Qiu, B. Gao, Effect of final annealing temperature on corrosion resistance of SZA-6 zirconium alloy cladding tubes, Mater. Sci. Forum 944 (2019) 488–498.

[104] J. Yang, U. Stegmaier, C. Tang, M. Steinbrück, M. Große, S. Wang, H.J. Seifert, High temperature Cr-Zr interaction of two types of Cr-coated Zr alloys in inert gas environment, J. Nucl. Mater. 547 (2021) 152806.

[105] U. Holzwarth, H. Stamm, Mechanical and thermomechanical properties of commercially pure chromium and chromium alloys, J. Nucl. Mater. 300 (2002) 161–177.

[106] V. Engelko, G. Mueller, A. Rusanov, V. Markov, K. Tkachenko, A. Weisenburger, A. Kashtanov, A. Chikiryaka, A. Jianu, Surface modification/alloying using intense pulsed electron beam as a tool for improving the corrosion resistance of steels exposed to heavy liquid metals, J. Nucl. Mater. 415 (2011) 270–275.

[107] K. Lambrinou, M. Verwerft, J. Vleugels, A. Weisenburger, C. Lorrette, Y. De Carlan, F. Di Fonzo, M. Barzoum, A. Kohyama, J. Marrow, Innovative accident-tolerant fuel cladding materials the h2020 il trovatore perspective, in: Proceedings of the Water Reactor Fuel Performance Meeting, 2017 Water Reactor Fuel Performance Meeting, 2017.

[108] L. Hu, C. Qiu, Y. Chen, H. Li, H. Liu, Influenceof laser energy density on interfacial diffusion bonding and surface density of chromium coating by multi-arc ion plating on zirconium alloy, Coatings 10 (2020) 565.

[109] D.J. Park, H.G. Kim, Y.I. Jung, J.H. Park, J.H. Yang, Y.H. Koo, Behavior of an improved Zr fuel cladding with oxidation resistant coating under loss-of-coolant accident conditions, J. Nucl. Mater. 482 (2016) 75–82.

[110] J. Krejčí, M. Ševeček, J. Kabátová,F. Manoch, J. Kočí, L. Cvrček, J. Málek, S. Krum, P. Šutta, P. Bublíková, ExperimentaL Behavior Of Chromium-based Coatings, (2018).

[111] M. Grujicic, C.L. Zhao, W.S. DeRosset, D. Helfritch, Adiabatic shear instability based mechanism for particles/substrate bonding in the cold-gas dynamic-spray process, Mater. Des. 25 (2004) 681–688.

[112] J. Arasteh, G.H. Akbari, M.H. Khazaei Feizabad, Production of nanostructure Zr–$ZrCr_2$–Cr composite via MA process and subsequent heat treatment, Mater. Manuf. Process. 35 (2020) 1877–1884.

[113] J. Ribis, A. Wu, J.C. Brachet, F. Barcelo, B. Arnal, Atomic-scale interface structure of a Cr-coated Zircaloy-4 material, J. Mater. Sci. 53 (2018) 9879–9895.

[114] A. Wu, J. Ribis, J.C. Brachet, E. Clouet, F. Leprêtre, E. Bordas, B. Arnal, HRTEM and chemical study of an ion-irradiated chromium/zircaloy-4 interface, J. Nucl. Mater. 504 (2018) 289–299.

[115] W. Sigle, S. Krämer, V. Varshney, A. Zern, U. Eigenthaler, M. Rühle, Plasmon energy mapping in energy-filtering transmission electron microscopy, Ultramicroscopy 96 (2003) 565–571.

[116] F.Laves, Theory of alloy phases, in: American Society for Metals, 1955.

[117] J. Zhu, C. Liu, P. Liaw, Phase stability and mechanical behavior of NbCr2-based Laves phases, Intermetallics 7 (1999) 1011–1016.

[118] W. Xiang, S. Ying, Reaction diffusion in chromium-zircaloy-2 system, China Nuclear Information Centre, CNIC-01562, (2001).

[119] L. Nicolai, R. de Tendler, Chromium diffusion in zircaloy-4, J. Nucl. Mater. 82 (1979) 439–443.

[120] H. Mehrer, Diffusion in solid metals and alloys, Landolt-Börnstein numerical data and functional relationships in science and technology, Group III, 26 (1990).

[121] K. Zeng, M. Hamalainen, R. Luoma, A thermodynamic assessment of the Cr-Zr system, Z. fur Metallkd. 84 (1993) 23–28.

[122] J. Heuer, G. Lucadamo, P. Zafred, SEM, EBSD, Characterization of cold-sprayed chromium coatings on Zircaloy-4, Microsc. Microanal. 26 (2020) 404–405.

[123] W. Gong, H. Zhang, C. Wu, H. Tian, X. Wang, The role of alloying elements in the initiation of nanoscale porosity in oxide films formed on zirconium alloys, Corros. Sci. 77 (2013) 391–396.

[124] G. Neumann, C. Tuijn, Self-diffusion and Impurity Diffusion in Pure Metals: Handbook of Experimental Data, Elsevier, 2011.

[125] J. Liu, Z. Cui, Z. Hao, D. Ma, J. Lu, Y. Cui, C. Li, W. Liu, S. Xie, P. Hu, P. Huang, G. Bai, D. Yun, Steam oxidation of Cr-coated Sn-containing Zircaloy solid rod at 1000 °C, Corros. Sci. 190 (2021) 109682.

[126] N. Dupin, I. Ansara, C. Servant, C. Toffolon, C. Lemaignan, J.C. Brachet, A thermodynamic database for zirconium alloys, J. Nucl. Mater. 275 (1999) 287–295.

[127] A. Michau, M. Ougier, H. Maskrot, J.-C. Brachet, T. Guilbert, H. Palancher, J. Bischoff, E. Pouillier, Interlayers for Cr-coated nuclear fuel claddings: preliminary study of Mo, in: The Nuclear Materials Conference, Ghent, Belgium, 2020.

[128] A. Paz y Puente, J. Dickson, D.D. Keiser, Y.H. Sohn, Investigation of interdiffusion behavior in the Mo–Zr binary system via diffusion couple studies, Int. J. Refract. Met. Hard Mater. 43 (2014) 317–321.

[129] D.V. Sidelev, M.S. Syrtanov, S.E. Ruchkin, A.V. Pirozhkov, E.B. Kashkarov, Protectionof Zr alloy under high-temperature air oxidation: a multilayer coating approach, Coatings 11 (2021) 227.

[130] X. Wang, H. Guan, Y. Liao, M. Zhu, C. Xu, X. Jin, B. Liao, W. Xue, Y. Zhang, G. Bai, R. Wang, Enhancement of high temperature steam oxidation resistance of Zr–1Nb alloy with ZrO2/Cr bilayer coating, Corros. Sci. 187 (2021) 109494.

[131] J. Jiang, D. Zhan, J. Lv, X. Ma, X. He, D. Wang, Y. Hu, H. Zhai, J. Tu, W. Zhang, B. Wang, Comparative study on the tensile cracking behavior of CrN and Cr coatings for accident-tolerant fuel claddings, Surf. Coat. Technol. 409 (2021) 126812.

[132] A. Hellouin de Menibus, J. Sercombe, Q. Auzoux, C. Poussard, Thermomechanical loading applied on the cladding tube during the pellet cladding mechanical interaction phase of a rapid reactivity initiated accident, J. Nucl. Mater. 453 (2014) 210–213.

[133] J. Jiang, H. Zhai, P. Gong, W. Zhang, X. He, X. Ma, B. Wang, In-situ study on the tensile behavior of Cr-coated zircaloy for accident tolerant fuel claddings, Surf. Coat. Technol. 394 (2020) 125747.

[134] J. Jiang, M. Yuan, M. Du, X. Ma, On the crack propagation and fracture properties of Cr-coated Zr-4 alloys for accident-tolerant fuel cladding: In situ three-point bending test and cohesive zone modeling, Surf. Coat. Technol. (2021) 127810doi: https://doi.org/127810.121016/j.surfcoat.122021.127810.

[135] Z. Xu, J. Wei, Y. Liu, B. Wang, The effect of oblique crack on stability and fracture properties of Cr-coated Zircaloy cladding, Ann. Nucl. Energy 163 (2021) 108560.

[136] H. Cheng, G. Chen, Z. Zhang, X. Chen, Uniaxial ratcheting behaviors of Zircaloy-4 tubes at 400 °C, J. Nucl. Mater. 458 (2015) 129–137.

[137] D.C. Roache, A. Jarama, C.H. Bumgardner, F.M. Heim, J. Walters, J. Romero, B. Maier, X. Li, Unveiling damage mechanisms of chromium-coated zirconium-based fuel claddings by coupling digital image correlation and acoustic emission, Mater. Sci. Eng. A 774 (2020) 138850.

[138] J. Jiang, M. Du, Z. Pan, M. Yuan, X. Ma, B. Wang, Effects of oxidation and inter-diffusion on the fracture mechanisms of Cr-coated Zry-4 alloys: an in situ three-point bending study, Mater. Des. (2021) 110168doi: https://doi.org/110110.111016/j.matdes.112021.110168.

[139] P. Červenka, J. Krejčí, L. Cvrček, V. Rozkošný, F. Manoch, D. Rada, J.J.A.P.C.P. Kabátová, Experimental study of damaged Cr-coated fuel cladding in post-accident conditions, Acta Polytechnica CTU Proceedings 28 (2020) 1-7.

[140] B. Boyack, A. Motta, K. Peddicord, C. Alexander, J.J.N.C.-. Andersen, LA-UR-00-, Phenomenon identification and ranking tables(PIRTs) for loss-of-coolant accidents in pressurized and boiling water reactorscontaining high burnup fuel, Los Alamos National Laboratory, (2001).

[141] J. Stuckert, M. Große, C. Rössger, M. Klimenkov, M. Steinbrück, M. Walter, QUENCH-LOCA program at KIT on secondary hydriding and results of the commissioning bundle test QUENCH-L0, Nucl. Eng. Des. 255 (2013) 185–201.

[142] J. Stuckert, M. Grosse, M. Steinbrueck, M. Walter, A. Wensauer, Results of the QUENCH-LOCA experimental program at KIT, J. Nucl. Mater. 534 (2020) 152143.

[143] J. Hazan, A. Gauthier, E. Pouillier, K. Shirvan, Semi-integral LOCA test of cold-spray chromium coated zircaloy-4 accident tolerant fuel cladding, J. Nucl. Mater. 550 (2021) 152940.

[144] J. Brachet, M. Le Saux, V. Lezaud-Chaillioux, M. Dumerval, Q. Houmaire, F. Lomello, F. Schuster, E. Monsifrot, J. Bischoff, E. Pouillier, Behavior under LOCA conditions of enhanced accident tolerant chromium coated zircaloy-4 claddings, in: Proceedings of the TopFuel Conference, Boise, ID, USA, 2016.

[145] X. Ma, H. Zhai, F. Meng, J. Jiang, X. He, Y. Hu, W. Zhang, J. Tu, D. Wei, B. Wang, Benefit or harm of accident tolerant coatings on the low-cycle fatigue properties of Zr-4 cladding alloy: in-situ studies at 400 °C, J. Nucl. Mater. 545 (2021) 152651.

[146] B. Reed, R. Wang, R.Y. Lu, J. Qu, Autoclave grid-to-rod fretting wear evaluation of a candidate cladding coating for accident-tolerant fuel, Wear 466–467 (2021) 203578.

[147] F. D'Auria, M. Dusic, L. Dutton, C. Fry, H. Glaeser, G. Kim, I.H. Lee, S.B. Mavko, F. Pelayo, A. Petruzzi, Deterministic safety analysis for nuclear power plants, IAEA Specific Safety Guide, IAEA, 2009.

[148] J.-O. Andersson, Thermodynamic properties of chromium, Int. J. Thermophys. 6 (1985) 411–419.

[149] R.F. Domagala, D.J. McPherson, System zirconium-oxygen, JOM 6 (1954) 238–246.

[150] C. Tang, M. Grosse, M. Steinbrueck, K. Shirvan, Oxidation and quench behavior of cold spraying Cr-coated zircaloy fuel cladding under severe accident scenarios, in: Proceedings of the Int. Nuclear Fuel Cycle Conf. (TOP FUEL 2019), 2019, 22–26.

[151] J. Liu, C. Tang, M. Steinbrück, J. Yang, U. Stegmaier, M. Große, D. Yun, H.J. Seifert, Transient experiments on oxidation and degradation of Cr-coated Zircaloy in steam up to 1600 °C, Corros. Sci. 192 (2021) 109805.
[152] H.-B. Ma, Y.-H. Zhao, Y. Liu, J.-T. Zhu, J. Yan, T. Liu, Q.-S. Ren, Y.-H. Liao, G. Liu, X.-D. Lin, M.-Y. Yao, Self-healing behavior of Cr-coated Zr alloy cladding in high temperature steam oxidation process, J. Nucl. Mater. 558 (2022) 153327.
[153] Z. Xu, Y. Liu, B. Wang, Effect of initial coating crack on the mechanical performance of surface-coated zircaloy cladding, Nucl. Eng. Technol. 53 (2021) 1250–1258.
[154] D.J. Young, High Temperature Oxidation and Corrosion of Metals, Elsevier, 2008.
[155] A. Michau, F. Maury, F. Schuster, F. Lomello, J.C. Brachet, E. Rouesne, M. Le Saux, R. Boichot, M. Pons, High-temperature oxidation resistance of chromium-based coatings deposited by DLI-MOCVD for enhanced protection of the inner surface of long tubes, Surf. Coat. Technol. 349 (2018) 1048–1057.
[156] M. Steinbrück, J. Birchley, A.V. Boldyrev, A.V. Goryachev, M. Grosse, T.J. Haste, Z. Hózer, A.E. Kisselev, V.I. Nalivaev, V.P. Semishkin, L. Sepold, J. Stuckert, N. Vér, M.S. Veshchunov, High-temperature oxidation and quench behaviour of Zircaloy-4 and E110cladding alloys, Prog. Nucl. Energy 52 (2010) 19–36.
[157] R. Guillou, M. Le Saux, E. Rouesne, D. Hamon, C. Toffolon-Masclet, D. Menut, J. Brachet, J. Bechade, D. Thiaudiere, In-situ time-resolved study of structural evolutions in a zirconium alloy during high temperature oxidation and cooling, Mater. Charact. (2019) 109971.
[158] D. Sidelev, S. Ruchkin, E. Kashkarov, High-temperature oxidation of Cr-coated resistance upset welds made from E110 alloy, Coatings 11 (2021) 577.
[159] X. Dong, X. Fang, X. Feng, K.-C. Hwang, Diffusion and stress coupling effect during oxidation at high temperature, J. Am. Ceram. Soc. 96 (2013) 44–46.
[160] N. Lakshmi, H.I. Yoo, M. Martin, Oxidation kinetics of zirconium examined by in situ X-ray diffraction, J. Electrochem. Soc. 160 (2013) C136–C141.